Design of new Cu-Fe metallic oxide foams formed by electrodeposition for asymmetric supercapacitors electrodes

Grzegorz Adam Lange

Thesis to obtain the Master of Science Degree in

Energy Engineering and Management

Examination committee

Chairperson: Prof. José Alberto Caiado Falcão de Campos

Supervisors: Prof. Maria de Fátima Grilo da Costa Montemor

Dr Sónia Cristina da Conceição de Matos Eugénio

Dr inż. Wojciech Zając

Members of the commitee: Maria Teresa Oliveira de Moura e Silva

February 2014

Acknowledgements

This thesis is based on work conducted within the KIC InnoEnergy Master School, in the MSc program Clean Coal Technologies. This program is supported financially by the KIC InnoEnergy. The author also received financial support from KIC InnoEnergy, which is gratefully acknowledged.

KIC InnoEnergy is a company supported by the European Institute of Innovation and Technology (EIT), and has the mission of delivering commercial products and services, new businesses, innovators and entrepreneurs in the field of sustainable energy through the integration of higher education, research, entrepreneurs and business companies. Shareholders in KIC InnoEnergy are leading industries, research centres, universities and business schools from across Europe.

The Clean Coal Technologies MSc program is a collaboration of:
AGH University of Science and Technology, Kraków, Poland,
SUT Silesian University of Technology, Gliwice, Poland,
IST Instituto Superior Técnico , Lisbon, Portugal.

Acknowledgements

I would like to express my gratitude to Prof. Fátima Montemor, my supervisor at Instituto Superior Técnico, for helpful advices and support during the course of this work.

I would like to express the deepest appreciation to Dr Sónia Eugénio, my co-supervisor at Instituto Superior Técnico, for all her orientation, availability and fresh look at dissertation. Without her continuous help during laboratory research this work would not have been possible.

I am also thankful to Dr inż. Wojciech Zając, my supervisor at AGH University of Science and Technology, for his support, technical hints and kindness.

I want to thank all my colleagues from Grupo de Estudos de Corrosão e Efeitos Ambientais of IST, especially Rui and Miguel, for help and generosity during laboratory research.

Abstract

Increased energy demand is a worldwide phenomenon driven by factors such as industrialization, growth of economies and increased mobility of people. Hence, the rational consumption of energy and the efficient use of renewable energy sources have become key issues that depend strongly on the development of high performance energy storage systems. In this context, supercapacitors have attracted special attention as unique devices comprising high power density, long cycling life as well as short charge/discharge time. Despite a disadvantage in terms of energy density comparatively to batteries, supercapacitors are nowadays considered as the most promising innovation in the energy storage area. The performance of a supercapacitor is defined by the material that is used as electrode. Therefore, the development of new electrodes is one of the most challenging areas towards the development of advanced supercapacitors. In this field, transition metal oxides are becoming very attractive materials because of their pseudocapacitive electrochemical behavior. Many different materials and production routes are currently available, but many of them are not adequate to scale up because of the cost of the process. Therefore, nowadays the challenge is to fabricate cheap but effective electrodes for supercapacitors based on routes with potential of large scale production. The electrodeposition process is a very versatile and cheap method for the production of new transition metallic oxide electrodes having high capacity and high performance. In the present work, Cu-Fe nanostructured foams were produced by electrodeposition directly on current collectors. The influence of the electrodeposition parameters on the morphology and electrochemical response of the produced electrodes was studied in detail. For this purpose, the morphology and the chemical composition of produced foams were studied by scanning electron microscopy (SEM) and energy dispersive spectroscopy (EDS), respectively. The selected samples were also studied by X-ray diffraction (XRD). The electrochemical response was assessed by cyclic voltammetry and charge-discharge (chronopotentiometry) experiments. For further optimization, a set of selected samples was subjected to heat treatment at various temperatures. The heat treatment at 150 °C resulted in specific capacitances of 205 Fg^{-1}. The samples were submitted to a long term test, during which they were charged and discharged 8000 times. The results demonstrate approximately 33.5 % of capacitance loss. Given the working potential windows of these materials they are suitable to work as negative electrodes in asymmetric supercapacitor configurations.

Keywords: supercapacitors, specific capacitance, electrodeposition, cyclic voltammetry, charge-discharge curves.

Resumo

A crescente necessidade energética é um fenómeno mundial motivado por diversos fatores como a industrialização, crescimento económico e transportes. Assim, o consumo racional de energia e a utilização de energias renováveis tornaram-se temas prioritários, que dependem fortemente do desenvolvimento de sistemas de armazenamento de energia inovadores e alternativos. Neste contexto, os supercondensadores têm atraído bastante atenção como dispositivos de elevada densidade de potência, longo tempo de vida e tempo curto de carga/descarga. Apesar de alguma desvantagem em termos de densidade de energia quando comparados com baterias, os supercondensadores são atualmente considerados a inovação mais promissora na área do armazenamento de energia. O desempenho dos supercondensadores é definido pelo material que é utilizado como elétrodo. Assim, o desenvolvimento de novos elétrodos é uma das áreas mais desafiantes para o desenvolvimento de supercondensadores avançados. Neste campo, os óxidos de materiais de transição têm-se tornado materiais atrativos devido ao seu comportamento eletroquímico pseudo-capacitivo. Existem atualmente diferentes materiais e métodos de produção mas muitos não são adequados para industrialização devido ao elevado custo do processo. Por isso, atualmente, o maior desafio é fabricar elétrodos para supercondensadores que sejam baratos mas eficientes, através de processos passíveis de aplicação em produção a larga escala. A electrodeposição é um processo muito versátil e de baixo custo para a produção de novos elétrodos de óxidos de metais de transição com elevada capacidade e desempenho. No presente trabalho, espumas metálicas nano-estruturadas de ferro-cobre foram produzidas por electrodeposição direta em coletores de corrente. A influência dos parâmetros de deposição na morfologia e resposta eletroquímica dos elétrodos produzidos foi estudada em detalhe. Com este objetivo, a morfologia e composição química das espumas produzidas foram estudadas por microscopia eletrónica de varrimento (SEM) e espectroscopia de energia dispersiva de raios-X (EDS), respetivamente. Amostras selecionadas foram também analisadas por difração de raios-X (XRD). A resposta eletroquímica foi avaliada por voltametria cíclica e curvas de carga-descarga (cronopotenciometria). Posteriormente, uma série de amostras selecionadas sofreram tratamento térmico a várias temperaturas. O tratamento a 150 °C resultou em capacidades específicas de 205 Fg^{-1}. As amostras foram também submetidas a testes de longa duração, durante os quais foram carregadas e descarregadas 8000 vezes. Os resultados mostraram uma perda de capacidade de aproximadamente 33.5 %. Tendo em conta a janela de potencial destes materiais, estes são apropriados para aplicação como elétrodos negativos em supercondensadores com configuração assimétrica.

Palavras-chave: supercondensadores, capacidade especifica, eletrodeposição, voltametria cíclica, curva de carga-descarga.

Abstrakt

Zwiększone zapotrzebowanie na energię elektryczną jest zjawiskiem ogólnoświatowym, które jest związane z takimi czynnikami jak wzrost uprzemysłowienia czy intensyfikacja transportu. Produkcja nowych urządzeń elektronicznych, zmiany w przemyśle czy rozwój krajów silnie zależą od alternatywnych i innowacyjnych systemów magazynowania energii. Superkondensatory wydają się być bardzo atrakcyjnym wariantem ze względu na takie cechy jak wysoka gęstość mocy, długa żywotność oraz krótki czas samego procesu ładowania. Pomimo stosunkowo niskiej gęstości energii, superkondensatory uważane są za najbardziej obiecujące i innowacyjne magazyny energii. Wydajność superkondensatora jest określona przez materiał zastosowany jako elektroda. Z tego względu, rozwój nowych materiałów elektrodowych bezpośrednio wpływa na przyszłość superkondensatorów. Dużą uwagę przyciągnęły tlenki metali posiadające właściwości pseudopojemnościowe. Obecnie dostępnych jest wiele materiałów oraz metod produkcji, jednak wiele z nich nie może być zastosowanych na większą skalę z uwagi na wysokie koszty. Dlatego też prowadzone są badania nad wytwarzaniem tanich i skutecznych elektrod dla potrzeb superkondensatorów. Proces elektrochemicznego nanoszenia powłok jest uniwersalną i tanią metodą produkcji elektrod złożonych z tlenków metali posiadających duże pojemności i wydajności. W niniejszej pracy za pomocą tej metody otrzymano porowate struktury Cu-Fe. Zbadano wpływ parametrów elektrochemicznego nakładania powłok na morfologię i właściwości elektrochemiczne wyprodukowanych elektrod. W tym celu użyto mikroskopii skaningowej (SEM) oraz dyspersyjnej spektroskopii rentgenowskiej (EDS) w celu identyfikacji otrzymanych struktur, jak również poznania ich składu chemicznego. Wybrane próbki zostały poddane badaniu rentgenografii strukturalnej (XRD). Badania elektrochemiczne przeprowadzono za pomocą woltamperometrii cyklicznej oraz cykli ładowań i rozładowań (chronopotencjometria). Zastosowanie temperatury 150 °C pozwoliło na otrzymanie przez jedną z próbek pojemności właściwej rzędu 205 Fg^{-1}. Przeprowadzono również test stabilności otrzymanych struktur podczas którego próbka poddana została 8000 cyklom ładowań i rozładowań czego wynikiem był spadek pojemności właściwej o około 33.5%. Po zadaniu napięcia pracy, otrzymany materiał może być zastosowany w roli ujemnej elektrody w superkondensatorach asymetrycznych.

Słowa kluczowe: superkondensator, pojemność właściwa, elektrochemiczne nanoszenie powłok, woltamperometria cykliczna, krzywe ładowania-rozładowania.

Table of content

1. Introduction 19

2. Supercapacitors 21

2.1. Types of capacitors 21

2.2. Comparison with other energy storage devices 25

2.3. Materials used for electrodes 27

2.3.1. Carbon-based materials 27

2.3.2. Conductive polymers 28

2.3.3. Metal oxides 28

3. Nanoporous metallic foams 31

4. Properties of the produced materials 33

5. Fundamentals of electrodeposition 35

6. Methodology 39

6.1. Materials and solutions 39

6.2. Electrochemical set-up 40

6.3. Electrodeposition parameters 41

6.4. Thermal conditioning 42

6.5. Characterization techniques 42

6.5.1. Scanning electron microscopy (SEM) 42

6.5.2. Energy dispersive X-ray spectroscopy 43

6.5.3. X-ray diffraction 44

6.5.4. Cyclic voltammetry 45

6.5.5. Chronopotentiometry 46

7. Results and discussion 49

7.1. Optimization of electrodeposition parameters: electrolyte solution, applied current and deposition time 49

7.2. Morphology 52

7.2.1. Morphological characterization of the raw samples 52

7.2.2. Morphological characterization of the heat treated samples 55

7.2.3. Chemical composition of the metallic foams 57

7.2.4. Dependency of deposited mass on current density and deposition time 59

7.3. XRD analysis 59
7.4. Electrochemical characterization 60
7.4.1. Cyclic voltammetry results 60
7.4.2. Charge-discharge curves 63
7.4.3. Capacitance dependency on the number of cycles 66
8. Conclusions 69
9. Suggestions for future work 71
10. Bibliography 73

List of figures

Fig. 1. Presentation of electrostatic capacitor with description of elements. 21
Fig. 2. Polarization effect in electrostatic capacitor. 22
Fig. 3. Representation of electrolytic capacitor. 23
Fig. 4. Examples of ceramic capacitors. 23
Fig. 5. Model of electrical double-layer capacitor (ELDC). 24
Fig. 6. Ragone chart. 26
Fig. 7. Scheme showing hydrogen bubbling acting as template in the fabrication of a Cu foam deposited on gold substrates. 32
Fig. 8. The distribution of the ions and potential variation in the double layer. 36
Fig. 9. Typical electrodepositon setup. 37
Fig. 10. Stainless steel substrates used for electrodeposition 39
Fig. 11. Scheme of electrodeposition setup 40
Fig. 12. Substrates with deposited metals. 41
Fig. 13. Scheme of a scanning electron microscope. 43
Fig. 14. XRD technique and conversion of d-spacings to diffraction pattern. 45
Fig. 15. Example of a cyclic voltammogram. 45
Fig. 16. SEM images (of films electrodeposited at 3A for 180 s from (a) - solution no. 2, (b) - solution no. 3, (c) - solution no. 7, (d) - solution no. 9. 50
Fig. 17. Fig. 17. SEM images of films electrodeposited from solution 5 at 0.825 A and 90 s (a), 1.65 A and 90 s (b), 0.825 A and 180 s (c) and 1.65 A and 180 s (d). 51
Fig. 18. SEM images of Cu-Fe deposits for sample 90s_2.475A at different magnifications: a) 200x, b) 500x, c) 1000x, d) 5000x. 53
Fig. 19. SEM images of Cu-Fe deposits for sample 90s_3A at different magnifications: a) 200x, b) 500x, c) 1000x, d) 5000x. 54
Fig. 20. SEM images of Cu-Fe deposits for sample 180s_3A at different magnifications: a) 200x, b) 500x, c) 1000x, d) 5000x. 54
Fig. 21. SEM images of metallic foam deposited at 2.475 A for 90 s (a, d) as is and after heat treatment at (b, e) 150 ^{o}C and (c, f) 250 ^{o}C. 55
Fig. 22. SEM images of metallic foam deposited at 3 A for 90 s (a, d) as it is and after heat treatment at (b, e) 150 ^{o}C and (c, f) 250 ^{o}C. 56
Fig. 23. SEM images of metallic foam deposited at 3 A for 180 s (a, d, g) as it is and after heat treatment at (b, e, h) 150 ^{o}C and (c, f, i) 250 ^{o}C. 57
Fig. 24. EDS spectrum of metallic foam obtained at 2.475 A for 90 s. 58
Fig. 25. Variation of Cu and Fe content of the foams with the deposition parameters. 58
Fig. 26. Relationship between deposit mass and applied current density. 59
Fig. 27. Diffractograms of Cu-Fe foams obtained at 3A current and 180s before and after heat treatment 60

Fig. 28. Typical peaks occurring in the voltammograms. Sample 90s_2.475A_150C. Scan rate 50 mV/s..... 61
Fig. 29. Cyclic voltammograms of Cu-Fe foams deposited in different conditions in 1 M NaOH. Scan rate 50 mV/s. 62
Fig. 30. Cyclic voltammograms of Cu-Fe foams before and after heat treatment in 1 M NaOH. Scan rate 50 mV/s. 63
Fig. 31. Typical charge-discharge curves obtained for sample 90s_2.475A. Applied charge and discharge current is equal +1 mA/cm^2 and -1 mA/cm^2, respectively. 64
Fig. 32. Raw samples discharge curves comparison. Discharge current is equal -1 mA/cm^2. 64
Fig. 33. Comparison of charge-discharge curves of raw and heat treated samples obtained in 90s and 2.475A current. 66
Fig. 34. Capacitance dependency on number of cycles (vs. SCE). 66

List of tables

Tab. 1. Comparison of properties of batteries, electrostatic capacitors and electrochemical capacitors. 27
Tab. 2. Comparison of some properties of the metals used in this work for the electrodeposition of the metallic foams..... 33
Tab. 3. Application of different alloys that can be deposited by plating. 37
Tab. 4. Chemical composition of AISI 304 stainless steel 39
Tab. 5. Electrolytes used for electrodeposition. 40
Tab. 6. Variation of applied current and time of electrodeposition. 41
Tab. 7. X-ray lines of elements typically found in Cu-Fe NMFs. 44
Tab. 8. Results from electrodeposition experiments using different electrolyte solutions. 49
Tab. 9. Samples obtained from electrolyte 5..... 50
Tab. 10. Identification of raw samples selected for tests. 51
Tab. 11. Description of heat treated samples..... 52
Tab. 12. Peak potentials for Fe and Cu according literature. 62
Tab. 13. Values for specific capacitance obtained from the charge discharge curves. 65

1. Introduction

Technological developments that we are witnessing nowadays in the area of energy production and its rational use are creating and increasing pressure on the development of effective energy storage devices. Supercapacitors are, together with batteries, in the forefront of these developments. They found applications in a wide range of sectors, including growing markets associated with the automotive or electronic sectors where energy storage and efficient energy delivery are the main requirements for increased performance.

The year of 1972 proved to be a breakthrough in this area when the Japanese company Matsuhita Electric Industrial Co. (Osaka, Japan) used a carbon based material with high specific surface area to construct electrochemical capacitors, with higher capacitance than those known at that time. This new type of capacitor was called a supercapacitor. In addition, to the high electrical capacitance (order of even a few hundred Farads), supercapacitors are characterized by an energy density higher than conventional capacitors and a power density higher than that of batteries. The power density is associated with the fact, that the supercapacitor can receive/deliver large amounts of energy in a short period of time, i.e. charging and discharging with high currents in order to obtain fast charge exchange.

High energy and power densities are characteristics that define an energy storage device [1]. Comparatively to batteries, supercapacitors have a much lower market size, but the most recent developments point out that in the near future supercapacitors will play a major role as energy storage devices. Currently, supercapacitors due to constant upgrades are used for many purposes, which, among others, include:

- Storage in wind power stations - supercapacitors quickly adapt to changes in load. Such changes are always occurring in the wind turbines where the constant changes of weather and wind speed affects the production load. Fast response and high power density are required to deal with these changes and supercapacitors can provide the right support.

- Application in the household equipment and electronic tools, especially when fast response is required.

- In automotive industry supercapacitors are used in helping classical batteries as buffers, mainly during breaking. During this process, the energy is recovered by a supercapacitor, lowering the operating costs of the vehicle. They are used in hybrid and electric cars.

- Other applications include military industry, space and aeronautical (the emergency doors of the new airbuses are controlled by supercapacitors) industry, storage of energy produced in photovoltaic modules as well as in mobile devices.

The main highlights of supercapacitors are much higher energy density than capacitors, much higher power density than batteries and ability to sustain up to millions of charge/discharge cycles. The performance of supercapacitors is closely related to the properties of their electrode materials. Such electrodes must consist of high capacitance materials with a high surface area. The response of the electrode dictates the supercapacitor response and its ability to be used in a specific technical application. A great pressure is being imposed to the development of more effective and reliable electrodes for supercapacitors at affordable prices.

The aim of this research was to develop and to test new electrodes based on nanostructured metallic foams (NMFs) of Fe and Cu for application as redox supercapacitor electrodes. By combining properties characteristic of metals (good electrical and thermal conductivity) with a high surface area and ultralow density it is possible to obtain a promising electrode material for high performance supercapacitor.

2. Supercapacitors

2.1. Types of capacitors

In general, capacitors can be divided into three main groups:

1) Electrostatic
2) Electrolytic
3) Electrochemical supercapacitors
   a) Electrical double layer capacitor (*EDLC*)
   b) Redox (*pseudocapacitor*)

Electrostatic capacitors are constructed from a pair of conductors separated by a dielectric which may be air, mica or polymer film [2]. The dielectric is a non-conducting material, which is inserted between the parallel plates. When voltage is applied to the capacitor, the electrical energy from the power source is converted into electrostatic charge. Plate of the capacitor attached to the negative terminal of the power source accepts electrons while the second plate, connected with the positive terminal, loses electrons to the power source. As the flow of the current occurs, electrons are displaced in every part of the circuit. Once the capacitor is fully charged, the voltage across the plates is the same as the supply voltage and the charging current stops. As shown in Fig. 1, charges are placed on the plates of the capacitor creating an electrostatic field between them.

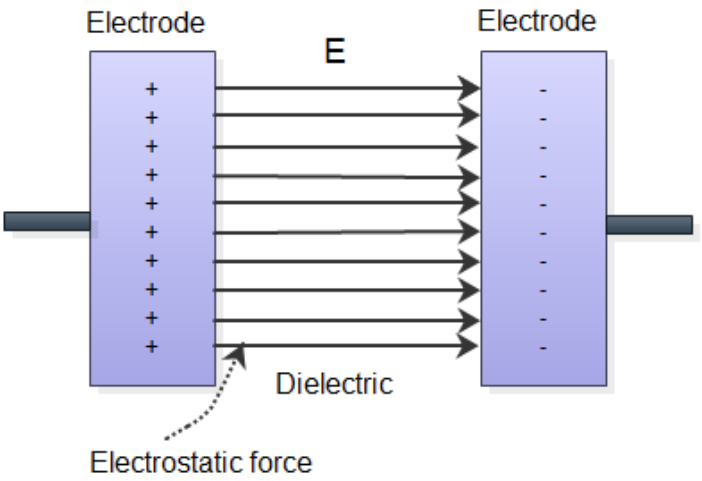

Fig. 1. Presentation of electrostatic capacitor with description of elements.

Adapted from [3] and [4]

The lines which flow from positive to negative charged plates represent the electrostatic field. In the situation where charges do not occur on the plates, the electrons move in circular way. If charge is stored, the electrons make elliptical movement due to the occurrence of the electrostatic

forces – electrons are attracted to the positive plate and repulsed by the negative plate. The above mentioned behavior of capacitor is related to the polarization effect which is shown in Fig. 2.

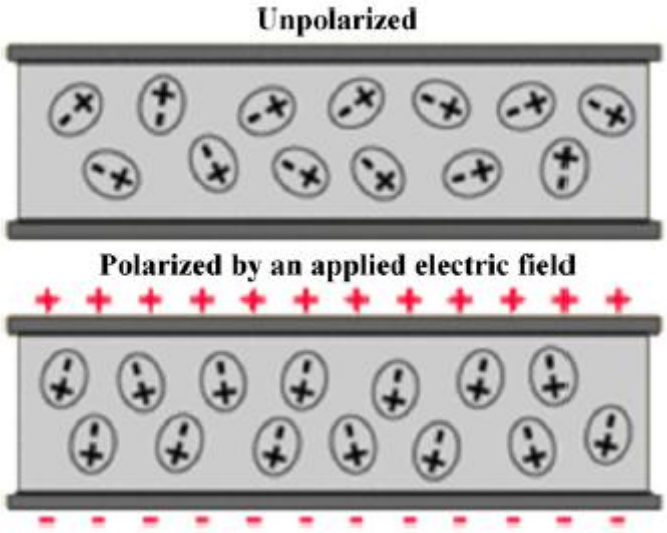

Fig. 2. Polarization effect in electrostatic capacitor.

Adapted from [3]

Electrostatic capacitors typically present low energy density (charge that the device is able to store) among the three types and the highest power density. They operate at gigahertz frequencies and have charge times around 10^{-6} s.

Another group of capacitors are the electrolytic capacitors, which are widely commercialized and find applications in many areas. Their construction is similar to that of electrostatic capacitors, but there is a conductive electrolyte between the plates in direct contact with the electrodes. Electrolytic capacitors can store 10 times more energy than the electrostatic capacitors and they may be used in frequencies up to 20 kHz [3]. An aluminum electrolytic capacitor (Fig. 3) contains an anode foil, a cathode foil separated by a dielectric film, usually fabricated through anodizing Al foil in boric acid solutions. The layer of Al_2O_3 (Fig. 3) has thickness of 1 μm and can endure a voltage of 700 V so that the capacitor may be applied in high voltages and thus prevent from flashover. Electrolytic aluminum capacitors are commonly used as power supplies in automotive industry, computers, motherboards and other electronic equipment.

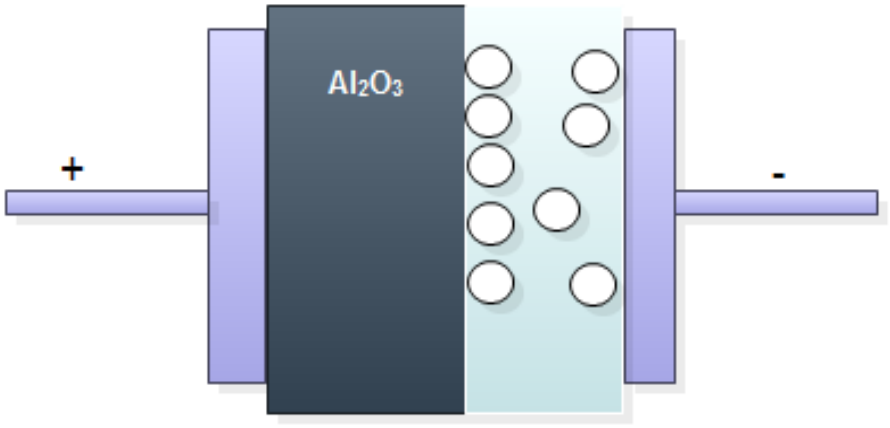

Fig. 3. Representation of electrolytic capacitor.

Adapted from [4]

In the case of tantalum electrolytic capacitors two types may be distinguished: wet electrolytic capacitors which use sulfuric acid as the electrolyte and solid electrolytic capacitors where MnO_2 plays the role of solid electrolyte. The capacitance of these devices ranges between 0.1 and 10 μF and voltage profiles of 25 to 50 V [4]. Capacitances obtained both in tantalum and aluminum capacitors are the same, the first type being characterized with higher temperature resistance and frequency. Furthermore, tantalum capacitors are usually chosen for circuits where high stability is required.

The last subgroup of electrolytic capacitors includes the ceramic capacitors. Capacitor presented in Fig. 4. is constructed of metal and ceramic, the ceramic material acts as the dielectric. Most commonly used are multilayer capacitors which usually consist of approximately 100 layers of electrode and dielectric ceramics. These layers are placed between two ceramic cover layers. Typically Ag-Pd is used as the electrode material and $BaTiO_3$ as the dielectric ceramics [4]. They may operate in the range of 10 μF and are widely used in high frequency applications.

Fig. 4. Examples of ceramic capacitors.

Adapted from [5]

Ceramic capacitors (Fig. 4) capacitors are very popular and found applications in areas such as transmitter stations, high voltage laser power supplies, induction furnaces or printed circuit boards [5].

Electrochemical capacitors bridge the gap between the batteries and conventional capacitors. They have much higher energy density than previously mentioned capacitors. They also offer a number of properties that make them very competitive comparing to other energy storage devices such as: fast charge/discharge cycles (range of seconds), long-term stability up to more than 500,000 cycles and ability to deliver ten times more power (higher power density) than batteries [9].

There are two classes of electrochemical capacitors: electrical double-layer capacitors and pseudocapacitors. Each class is characterized by its unique mechanism for storing charge. The former is based on non-faradaic charging of double-layer, while the latter is based on faradaic reactions. Electrochemical capacitors use electrolyte solutions and their high capacitance results from the porous electrode structure and occurrence of faradaic and non-faradaic reactions. As consequence, supercapacitors have better performance when compared to electrolytic and electrostatic capacitors [2].

The working principle of electrical double-layer capacitors (EDLCs) is based on a non-faradaic principle. Thus, the electric charges are accumulated on the electrode surfaces, while ions of opposite charge are present on the electrolyte side [10]. Electrical double layer capacitors are based on carbon materials. Carbon is a low cost, readily available material with high specific surface area that can reach 2500 m^2/g [6]. The scheme of an EDLC is presented in the Fig. 5.

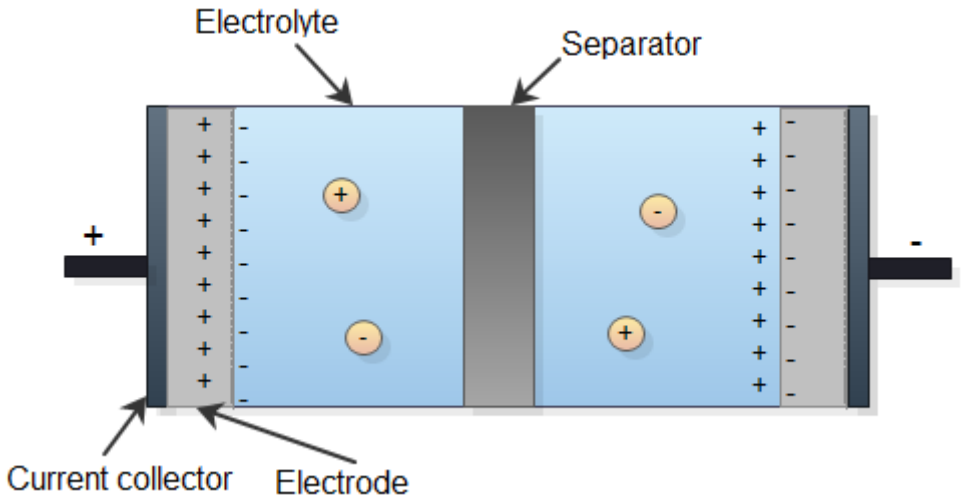

Fig. 5. Model of electrical double-layer capacitor (EDLC).

Adapted from [4]

The above figure shows a schematic view of an EDLC. There are two electrodes, made from the same material (e.g. activated porous carbon) and thus the device is symmetrical. The high capacitance results from the highly porous area of the electrode that results in the formation of a very effective double layer.

The selection of the electrode is one of the biggest challenges due to the necessity of high surface areas, suitable porosity, chemical and electrical compatibility with the electrolyte. A separator is placed between the electrodes, acting as a membrane, which allows the ions in the electrolyte to move through it. Additionally, it prevents the contact between the two carbon electrodes.

For enhanced EDLC performance the separator should be characterized by high electronic resistance, high ionic conductance and low thickness [8]. The electrolyte may be solid, organic or aqueous – the electrolyte type depends on the application of the capacitor. The nature of the electrolyte defines another important parameter: the working potential window of the electrode.

The electric current is transported by current collectors. EDLCs store energy in an electrochemical double layer which is formed at the solid/electrolyte interface. Positive and negative charges within the electrolyte accumulate at the surface of the electrode (solid) and compensate the charge at the electrode surface. The thickness of the accumulated layer is very small and depends on the concentration of ions. In addition, it is essential to increase the electrode area in contact with the electrolyte and this is why the increase of the electrode porosity is crucial for enhancing the energy stored by the supercapacitor electrodes [6]. The electrodes in EDLCs supercapacitors can display capacitances typically in the range of 100 – 200 Fg^{-1}. EDLCs can find many applications such as memory backup for timers, backup power sources when changing batteries, power sources that use solar cells such as watches and display lights or starters for small motors and cell motors.

The other subgroup of electrochemical supercapacitors are so called pseudocapacitors or faradaic supercapacitors. Here, the energy storage mechanism is based on faradaic processes, such as oxidation-reduction reactions, which involve electron transfer between the electrode and electrolyte of the supercapacitor. The process of charging/discharging is related to fast reversible redox reactions at the surface of the active material. Pseudocapacitance results from a number of electrosorption processes and redox reactions at the surface of oxide films covering a high surface area electrode [1]. Typically metallic oxides fall in this category.

The pseudocapacitor materials can increase the energy density due to the various reversible redox reactions that they may undergo. Using materials with high surface areas, the redox supercapacitors may display increased capacitance comparatively to EDLCs. On the other hand, and depending on the material used, the redox type electrodes can work in different potential windows. Thus, by combining suitable redox materials it is possible to work with different electrode configurations. This widens the potential operating window and creates an asymmetric configuration, in which the positive and negative electrode consists of distinct materials.

2.2. Comparison with other energy storage devices

Comparison of electrochemical capacitors (ECs) with other energy storage devices is commonly shown in Ragone plots as the one presented in Fig. 6. This diagram helps to characterize trade-offs for energy storage devices by comparing effective capacity and power handling. One look at the diagram explains why electrochemical capacitors gained considerable attention.

When compared to batteries and fuel cells, electrochemical capacitors present lower energy storage capability (energy density). The energy density of current commercial supercapacitors reaches 10 Wh/kg while in the case of common lead acid batteries this value is 30-35 Wh/kg, and more than 100 Wh/kg in lithium-ion batteries. On the other hand, supercapacitors have high rates of discharging and, as a consequence, high power density while fuel cells and batteries are characterized by longer times of charging/discharging. Therefore supercapacitors are complementary

to the other energy storage devices. Electrochemical capacitors are often used in combination with batteries in various applications in energy storage [12]. For example, if high energy density and high power density are required, the optimal solution seems to be combining batteries and supercapacitors devices in order to obtain more powerful systems.

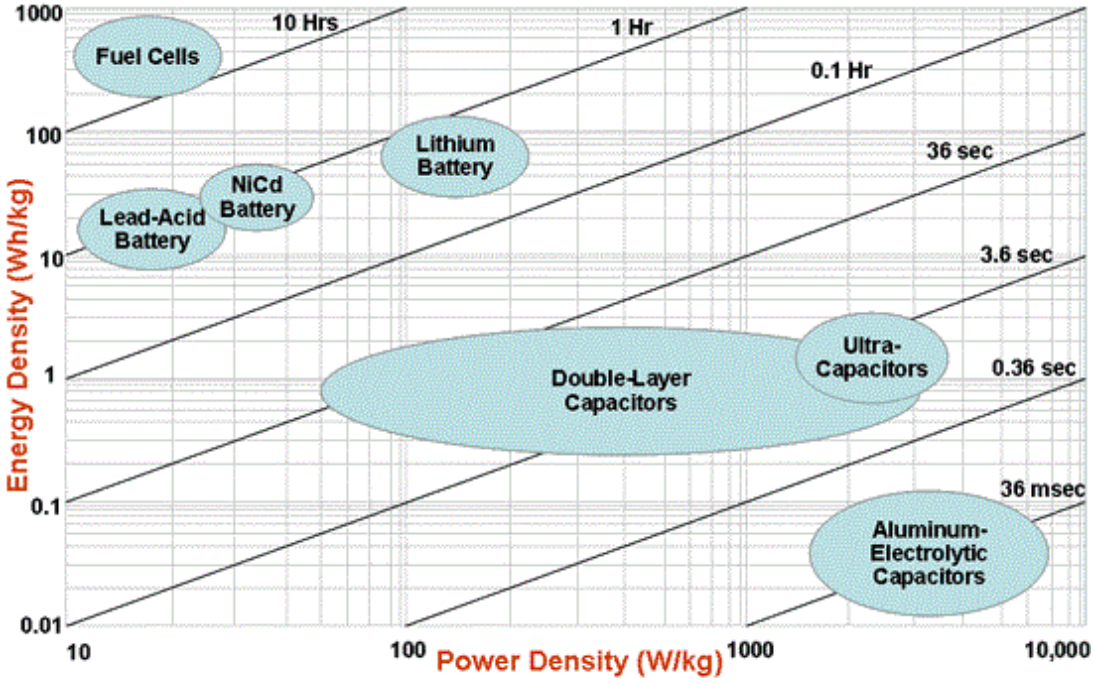

Fig. 6. Ragone chart.

Adapted from [11]

Some of the most relevant properties of supercapacitors in comparison with electrostatic capacitor and batteries are presented in Tab. 1. It may be seen, that electrochemical capacitors reach 10 times higher energy density when compared to electrostatic capacitors. Additionally they have the advantage of high power density, short charge-discharge times and very long lifecycle in comparison with batteries. This fact makes electrochemical capacitors the perfect device for filling the gap between capacitors and batteries. A fact worth mentioning is a relatively high charge-discharge efficiency observed for electrochemical capacitors which points on nearly zero loses in performance during its lifetime.

Tab. 1. Comparison of properties of batteries, electrostatic capacitors and electrochemical capacitors.

Adapted from [7]

	Battery	Electrostatic capacitor	Electrochemical capacitor
Discharge time	0.3 – 3 [h]	10^{-3} – 10^{-6} [s]	0.3 – 30 [s]
Charge time	1 – 5 [h]	10^{-3} – 10^{-6} [s]	0.3 – 30 [s]
Energy density [Wh/kg]	10 – 100	<0.1	1 – 10
Specific power [W/kg]	50 – 200	>10,000	~1000
Charge-discharge efficiency	0.70 – 0.85	~ 1	0.85 – 0.98
Cycle life	500 – 2000	>500,000	>100,000

2.3. Materials used for electrodes

2.3.1. Carbon-based materials

Carbon-based electrodes are widely used in EDLCs because of several factors that include: easy accessibility, relatively low cost, non-toxicity, wide temperature range applications and easy surface modifications [7]. A variety of carbons can be qualified as active materials in EDLCs electrodes, including high surface area activated carbons, carbon aerogels, carbon nanotubes (CNTs), template porous carbons, activated carbon nanofibers (CNFs) or activated carbon fabrics [13]. Carbons used in supercapacitors must have some relevant properties such as: *a)* a high specific surface area (range of 1000 – 2500 $m^2.g^{-1}$) to ensure high specific capacitance value, *b)* low resistivity and *c)* well adapted microtexture in order to allow good electrolyte accessibility into inner part of the surface of the electrode [14]. Carbon based electrodes are obtained by coating metallic current collectors with a mixture of activated carbon powder, conductive carbon black and organic binders. Generally, the specific capacitance of carbon electrodes is proportional to their specific surface area, since the charge stored by the material depends on the surface area of carbon that is in contact with the electrolyte. Studies have shown, that activated carbon-based electrodes can attain specific capacitance values up to 300 Fg^{-1} while activated carbons and commercial CNTs can reach value of 150-200 Fg^{-1} [15].

2.3.2. Conductive polymers

Conducting polymers can be used as electrodes for redox electrochemical capacitors. Conductive polymers represent a group of low cost materials, having suitable morphology, sustaining fast doping-undoping processes and can be easily manufactured into electrochemical capacitors [7]. The most common polymers used as supercapacitor electrodes are polypyrrole (PPy), polyaniline (PAni) and derivatives of polythiopene (PTh). According to the literature, typical specific capacitance values are 750 Fg^{-1} (PAni), 620 Fg^{-1} (PPy) and 485 Fg^{-1} (PTh) [16]. Conductive polymers can undergo redox reactions that allow storing charge in the bulk. One disadvantage of conductive polymers is related to the fact that they do not sustain a high number of charge/discharge cycles. In general they sustain less than one thousand cycles because there are changes in their physical structure caused by doping-undoping of ions [16]. Currently, new organic and inorganic nano-composites consisting of conductive polymers and metallic oxides such as MnO_2 are being studied due to their good reproducibility during hundreds of polarization cycles and their high specific capacitances.

2.3.3. Metal oxides

Economic analysis shows that the total cost of a capacitor strongly depends on the selected electrode material and that this value may reach 90% of the device cost [6]. Due to this fact, there are numerous research works focused on the development of new electrode materials. Transition metal oxides and hydroxides or oxy-hydroxides are seen as very interesting candidates for new electrodes for redox electrochemical capacitors. This fact is related to their low resistance, which causes high specific power effect and thus their commercial application becomes very reasonable. Transition metal oxides are considered as the best candidates for electrodes for supercapacitors, because they have a variety of oxidation states which are relevant in case of redox charge transfer.

One of the most studied metal oxides is RuO_2. This crystalline or amorphous hydrous compound is a very promising material due to its high specific capacitance (close to 700 Fg^{-1}) which is related to surface reactions between Ru ions and hydrogen ions [17]. Electrodes made with this metal oxide present long life cycle, high conductivity and good chemical reversibility. However, RuO_2 presents high toxicity and very high cost. Moreover, it was shown that some forms of this oxide are very stable, leading to irreversible reactions that decrease the long term capacitive response. In order to increase the conductivity of the electrode and specific surface area, ruthenium oxides have been combined with other materials such as carbon nanotubes or graphene. The faradaic capacitance of RuO_2 and the high double layer capacitance response presented by carbon materials seems to be a good solution in terms of gaining higher specific capacitances.

Due to cost consideration in case of RuO_2, cheaper transition metal oxides such as MnO_2 have attracted much attention. This oxide has lower cost and is non-toxic, being therefore an attractive solution for the replacement of ruthenium oxides in supercapacitor electrodes [17]. Manganese oxides can present several oxidation states that create a pseudocapacitive behavior, which depends on factors such as structure of the oxides, valence of the species and porosity. Studies have shown, that

thin MnO_2 films exhibit specific capacitances of approximately 700 Fg^{-1} [18]. However, increasing film thickness results in decreasing specific capacitance due to low conductivity of MnO_2. In this way, the general values of specific capacitance range between 100 and 300 Fg^{-1}, which is far from the reported theoretical value of 1370 Fg^{-1} [18]. Nowadays, the new concept is to combine manganese oxide with carbon materials or conductive polymers. This can be done by applying an ultrathin layer of MnO_2 on the surface of a porous, high surface area and electronically conducting structure to minimalize the electron transport distance. Composites produced from MnO_2 and polyaniline (PAni) have already exhibited capacitances above 400 Fg^{-1} [19]. The biggest disadvantage of manganese oxide in case of application for supercapacitors electrodes is its poor longtime-cycle performance. After 1000 charge/discharge cycles, specific capacitance can be reduced by 20 % what is a difficulty when it comes to utilization in energy storage devices [17]. To overcome this problem and improve long-term cyclability, other transition metals such as nickel or cobalt with MnO_2 has been suggested and are currently studied [20].

An alternative to MnO_2 is provided by Ni and Co oxides. These oxides also display multiple oxidation states which is an important feature related to redox reactions occurring in pseudocapacitors. Cobalt oxide electrodes have good efficiency and long-term performance along with corrosion stability. It was reported that heat treated Co_3O_4 was able to reach 291 Fg^{-1} whereas $Co(OH)_2$ used a single electrode approached 280 Fg^{-1} [17]. In the case of Ni oxides, specific capacitance of NiO after heat treatment increased from 200 Fg^{-1} to 278 Fg^{-1} in KOH solution. Literature reports that increased temperature has a defect healing effect for this type of oxides [17]. Studies on Ni hydroxides have provided specific capacitance of $Ni(OH)_2$ equal 578 Fg^{-1} [21]. The desire of obtaining high specific capacitances has led to combining Ni oxides and hydroxides with CNTs, a strategy that resulted in values above 1700 Fg^{-1}. Specific capacitance of 900 Fg^{-1} was obtained for 2D layered Co_3O_4 flakes having high surface area and porosity [22]. A common combination consists of the use of mixed cobalt-nickel oxides, which are characterized by capacitances of 569 Fg^{-1} [23].

Among the transition metallic oxides, Fe oxide is a very promising candidate for supercapacitors mainly due to its low cost and environmental friendliness. Iron oxide films can be grown by using techniques such as electro-oxidation, sol-gel process, chemical precipitation, thermal decomposition, electrocoagulation, template and electrochemical deposition [24]. It has been reported, that the specific capacitance of Fe_3O_4 depends on the electrolyte anion species and surface area (dispersion of the oxide crystallites) [10]. Generally, Fe_3O_4 electrodes do not manifest such high specific capacitances as it happens for MnO_2 or RuO_2. Literature gives values of specific capacitance of 5 – 7 Fg^{-1}, whereas this value can be increased up to 100 Fg^{-1} by optimization of the porosity and crystallinity of deposited Fe_3O_4 structures [10]. Studies on combining Fe_3O_4 with carbon black (3 wt. % Fe_3O_4) have allowed to obtain the highest specific capacitance value: 510 Fg^{-1} [25]. According to literature, Fe_3O_4 when used as electrode shows relatively low capacitance values that are consequence of its low electrical conductivity, which does not enable effective ion diffusion. It is important to mention, that intensive studies were carried out on $Fe(OH)_3$ (iron(III) hydroxide) and FeO(OH) (ferric oxyhydroxide), resulting in specific capacitance values of approximately 400 Fg^{-1} [26].

The need of cheap transition metals has also brought attention to Cu oxides. Recently, copper oxide thin films have been obtained by techniques such as sol-gel, chemical deposition and electrochemical deposition [27]. Among these methods, CBD (chemical bath deposition) and electrochemical deposition seem to be very versatile methods. Here, the films can be deposited at low temperatures on a variety of substrates, while thickness of the layers can be controlled by bath chemical composition and deposition time. Moreover, the simplicity of those methods allow to low cost and ease in adaptation to large-scale production [28]. Studies on copper oxide films revealed that specific capacitances may vary between 6 Fg^{-1} to 43 Fg^{-1} [27, 28]. In order to improve these values it is possible to combine copper with other metals such as Fe or Ni to obtain alloys presenting higher capacitances.

Generally, the price is an important factor when selecting the appropriate metal oxide for the construction of electrodes for supercapacitors. Nowadays, MnO_2 is one of the cheapest materials, however it presents a major drawback, because its resistivity tend to increase with time, thus decreasing the efficiency of the electrode. Therefore, other metals showing higher theoretical capacitances, such as Ni, Co, Fe and Cu need to be explored for this application. Indeed, various technologies can be applied in order to develop metallic oxides with increased surface area, tailoring them for application as supercapacitor electrodes.

3. Nanoporous metallic foams

Nanoporous structures show very interesting morphologies making them good candidates for applications in catalysis, electrochemical sensors and energy storage devices, i.e. applications, in which high specific area is an important requirement.

Nanoporous metallic foams (NMFs) are usually 3D structures of pores and interconnected nano-ramified walls that present porosities higher than 50% as well as a wide pore size distribution. These properties make them very interesting materials for application as electrodes for supercapacitors. These nanostructured materials present an increased surface area for hosting the electrochemical reactions. Furthermore, active species can diffuse fast when NMFs are used. They also combine the above mentioned properties with characteristics of metals, such as good electrical and thermal conductivity and ductility/malleability [29].

In order to fabricate highly porous structures several methods are available, however only a few can be used to fabricate cheap structures. The most common one consists on de-alloying of one metal from the alloy and hard-template processes. In the first method one of the metals present in the alloy is preferentially dissolved, while the second method deals with deposition of a metal in the free spaces of the template left after the metal removal. However, these processes can be expensive and not very flexible. Furthermore, these processes involve a number of steps, which increases the price of the final product.

Electrodeposition belongs to one of the most flexible and cheapest methods for porous materials production. By applying the right potentials (or currents), a dynamic template can be obtained. Thus, for the production on NMFs by electrodeposition, the dynamic template is formed by hydrogen bubbling, which is a spontaneous process that occurs simultaneously with metal deposition at the substrate. The process is very fast and highly dynamic hydrogen bubbling facilitates fast fabrication of metallic foams. This process is considered as a low-cost method. Moreover, by electrodeposition, the NMFs can be easily formed on metallic substrates having high electronic conductivity which is an advantage in the case of supercapacitor electrodes (direct application of active material on the current collector) [29].

According to published studies [30], self-supported foams of copper and tin can be deposited from acid electrolytes on copper substrates when a high cathodic current is applied. The foam structure of deposited copper is closely related to the nucleation and evolution of hydrogen bubbles during process of electrodeposition. Hydrogen bubbles firstly form on the substrate and thus prevent the deposition of copper in those gaps. When gas evolution is continued, the metal ions grow between the gas bubbles. In this situation hydrogen bubbles behave as a negative dynamic template around which the metal grows as a foam structure, as shown in Fig. 7.

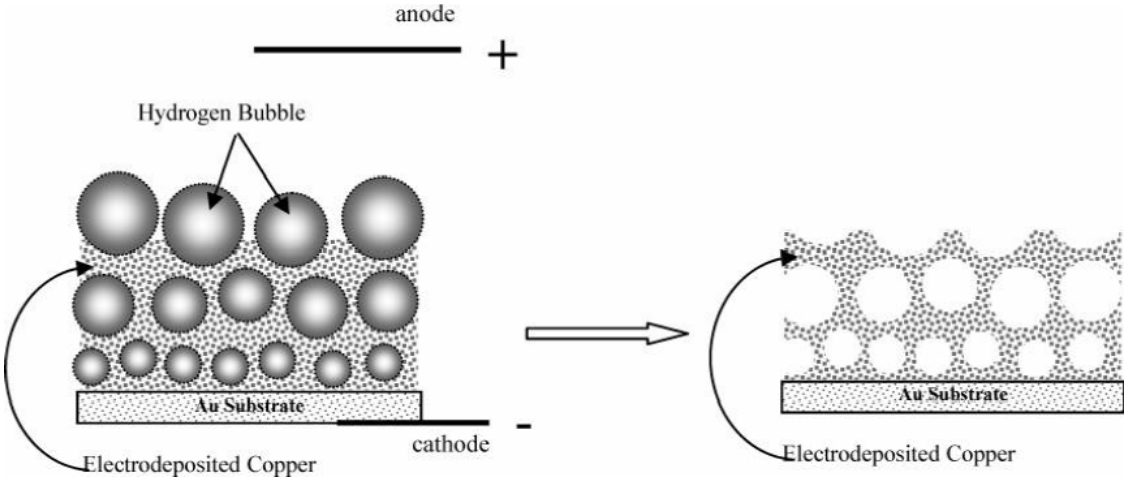

Fig. 7. Scheme showing hydrogen bubbling acting as template in the fabrication of a Cu foam deposited on gold substrates.

Adapted from [31]

Deposition parameters and electrolyte composition are crucial factors for the formation of porous metal foams on the substrate. The electrolyte composition can change the structure of pores (e.g. increased H_2SO_4 concentration in the electrolyte enhances hydrogen evolution and thus pore density is improved). On the other hand, the deposition time can lead to bigger pore size due to the hydrogen bubbles growth overtime [32]. It is also possible to control porosity by using additives, which act as bubble stabilizers and that avoid bubble coalescence or that have a catalytic effect on Cu deposition.

Not only copper, but also tin, silver, palladium and gold have been fabricated by means of electrodeposition using the dynamic hydrogen template technique. Furthermore, transition metals such as nickel and cobalt can be used to fabricate NMFs which seems to be a low-cost alternative to noble metals [32].

In the present work, iron-copper highly porous metallic foams were electrodeposited on stainless steel substrates applying the dynamic hydrogen bubble template for application as electrodes for supercapacitors. Low cost, good conductivity and high corrosion resistance are the main arguments which stand for choosing stainless steel substrate. This work studies the effect of the applied deposition time and current on the morphology and composition of Cu-Fe metallic foams as well as their electrochemical characterization in alkaline solution. Moreover, the work also aims at studying the effect of the heat treatment of the obtained foams and electrochemical response. The target is to characterize the properties of various Cu-Fe foams and their ability to be used as electrodes for supercapacitors.

4. Properties of the produced materials

In the present work Fe and Cu electrodeposited foams were studied. Crystalline ammonium iron (II) sulfate hexahydrate, $(NH_4)_2Fe(SO_4)2{\cdot}6H_2O$, was used as a precursor of iron - Fe^{2+}. This green salt is soluble in water, easily purified and more stable than other iron sulfates. In the case of Cu, crystalline copper (II) sulfate, $CuSO_4$, was studied.

Iron belongs to 8^{th} group of the periodic table, has an atomic number equal 26 and molar weight is 55.847 g/mol. The physical properties of iron strongly depend on its degree of purity. Iron is likely to form various forms of oxidized compounds and they have an acidic character which increases with increasing oxidation state. Iron in the metallic form is stable at room temperature, in dry air and in water that does not contain carbon dioxide or air (corrosion does not occur due to inhibited transformations of iron into iron oxyhydrate). Iron is abundant and its cost is not high comparatively to many other transition metals.

Tab. 2. Comparison of some properties of the metals used in this work for the electrodeposition of the metallic foams

Adapted from [33] and [34]

	Copper	Iron
Symbol	Cu	Fe
Atomic number	29	26
Density	8.89 [g/cm^3]	7.87 [g/cm^3]
Atomic weight	63.546 [u]	55.847 [u]
Electron configuration	[Ar] $4s^1 3d^{10}$	[Ar] $4s^2 3d^6$
Crystal structure	Face-centered cubic	Body-centered cubic Face-centered cubic
Oxidation states	+1, +2, +3, +4	+2, +3
Standard redox potential	$Cu^{2+} + 2e^- \leftrightarrow Cu$ 0.3402 [V] $Cu^{2+} + e^- \leftrightarrow Cu^+$ 0.5220 [V]	$Fe^{2+} + 2e^- \leftrightarrow Fe$ -0.4402 [V]
Melting point	1084.88 [°C]	1538.00 [°C]

Copper is one of the most widely used nonferrous metal. Copper's atomic number is 29, and the atomic mass equals 63.546 g/mol. Copper compounds are known in oxidation states which range from +1 to +4, but +2 (cupric) and +1 (cuprous) are the most common. In dry air and at room temperature copper slowly develops a thin film of copper (I) oxide, which plays a protective role. Pure copper is characterized by very good electrical and thermal conductivity performance, excellent workability and corrosion resistance. Properties of copper demonstrate strong dependence on temperature. Generally, increased temperature lowers the thermal conductivity. The same phenomenon occurs in the case of electrical conductivity. Parameters such as cold working or addition of elements that usually form solid solutions are important to increase the strength but may decrease the electrical conductivity. In general, the harder the copper, the lower its conductivity [34]. Copper has a wide range of applications. It is commonly used for electrical purposes like wires, rods, current generation devices, transformers and motors. About 40% of world consumption of copper is reserved for electrical purposes and almost 30% of world copper consumption is used for alloying [34]. Copper is also applied in many technical applications, including the chemical industry due to its resistance to corrosion.

5. Fundamentals of electrodeposition

Electrodeposition, also named electrochemical deposition or electroplating, refers to an electrochemical processes, through which a material is deposited on a conducting surface by reduction of cations present in solution, according to the following reaction [35]:

$$M^{z+} + ze^- \rightarrow M_{metal} \qquad \text{Eq. 1}$$

In general, the reduction reaction (Eq. 1) is induced by an external electric current (electrolytic processes) although, in some conditions, it may also occur spontaneously, without an external power supply (electroless processes).

Electrodeposition is widely used to apply thin homogeneous films on the surfaces of metallic substrates, with different purposes such as to improve corrosion resistance, increase abrasion resistance, improve decorative quality and surface conductivity. Electrodeposition is well known for many years and it has been used for a long time for decorative purposes and corrosion protection. Since the beginning of the last century many efforts have been made in order to optimize the electrodeposition and its application in order to improve the materials properties in many fields of science and industry, such as the automotive industry and the steel finishing industry.

According to Eq. 1, the deposition process occurs via the reduction reaction of charged species at the interface between the solid metal electrode and the liquid electrolyte. Basically, to perform electrodeposition it is necessary to have a setup consisting of electrodes (working and counter electrode), a power source (potentiostat/galvanostat), an electrochemical cell and the electrolyte inside. Electrodes are connected to a power source which controls the deposition process, i.e. voltage/current. The electrolyte is an ionic conductor, where the metal salt is dissolved in a suitable solvent [36]. The working electrode, which is the object to be plated and the counter electrode, usually made of an inert material (such as platinum or graphite), are immersed in the electrolyte and connected to the negative and positive terminals of the power supply, respectively. When an electric field is applied by the external power source across the working electrode, in order to pass the electrons to the ions contained in electrolyte, the uncharged elements or compounds are formed. Newly formed elements or compounds prefer to adhere at the surface of the working electrode than to remain in the electrolyte. In the present case, for Cu plating, the reactions occurring are as follows:

$$Cu^{2+} + 2e^- \leftrightarrow Cu_{metal} \qquad \text{Eq. 2}$$

$$2H_2O \leftrightarrow 4H^+ + O_2 + 4e^- \qquad \text{Eq. 3}$$

When the external potential is applied, the rearrangement of ions near the electrode surface occurs, resulting in the formation of a layer, which is known as the Helmholtz double layer. This process is followed by the formation of the diffusion layer, and these two layers are known as the Gouy-Chapman layer. The scheme of formation of the double layer is shown in Fig. 8. In the layer

closest to the surface, the distribution of charge occurs and potential changes linearly with the distance from the electrode surface. In the diffusion layer the potential changes exponentially.

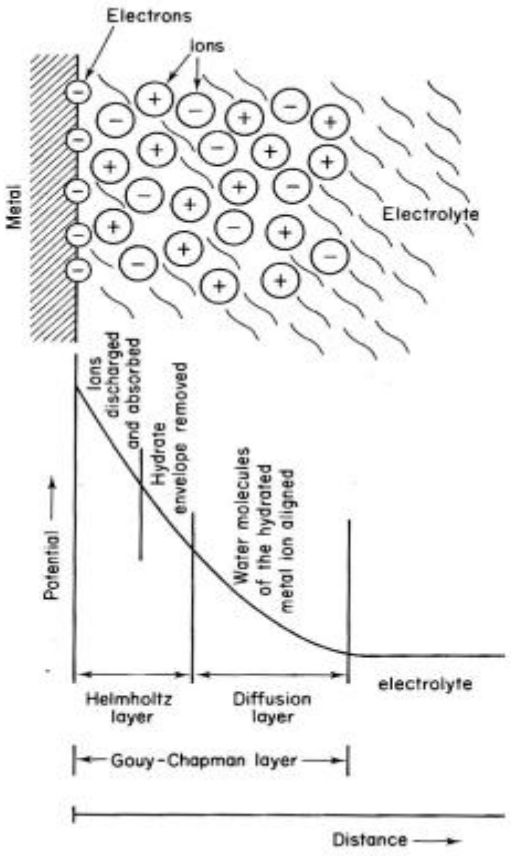

Fig. 8. The distribution of the ions and potential variation in the double layer.

Adapted from [37]

Hence, an electrode reaction is a sequence of various steps:

- Migration of hydrated metallic ions towards the cathode induced by the application of an external current
- Transfer of electrons at the cathode surface where a hydrated metal ion enters the diffused double layer. The water molecules are compensated in the diffused double layer. When metal ion enters the Helmholtz double layer, the hydrate envelope is removed
- Neutralization of the dehydrated ion and adsorption on the cathode surface
- In the case of electrodeposition, additional steps refers to the diffusion of the adsorbed atom to the growth point at the cathode surface and the formation of a new phase

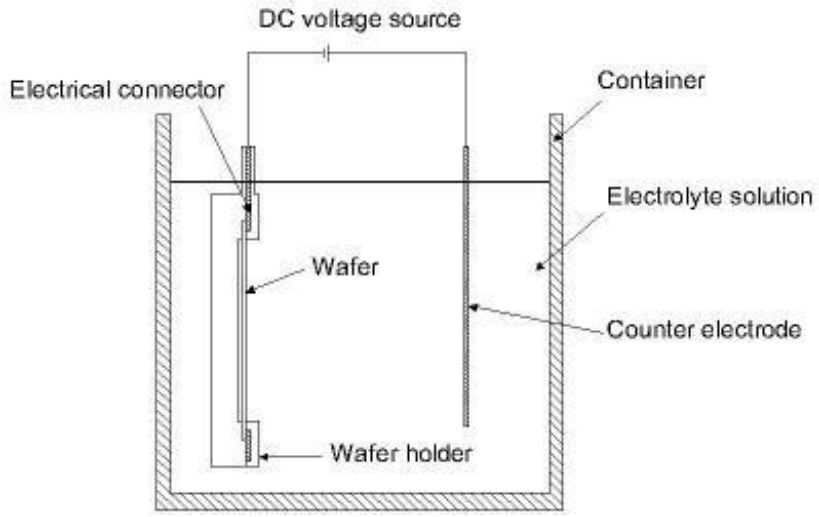

Fig. 9. Typical electrodepositon setup.

Adapted from [38]

The most common electrodeposition setup is presented in Fig. 9. Wafer is the object which is meant to be covered with the metal derived from the cations present in the electrolyte. As it was mentioned before, electrodeposition is a very attractive method in order to obtain homogeneous films of metals on metallic surfaces. Tab. 3 depicts some typical examples of alloys that can be deposited by plating on different metallic substrates for different purposes.

Tab. 3. Application of different alloys that can be deposited by plating.

Adapted from [36]

Alloy	Application
Ni-Zn, Ni-Au, Ni-Cd, Ni-Sn, Au-Cu, Au-Ag, Cu-Sn	Protection of surfaces, decorative function
Zn-Cd, Zn-Sn, Cd-Sn, Cr-Ni, Cr-Re	Corrosion resistance
Sn-Pb, Sn-Bi, Sn-Sb, Sn-Ni	Soldered coatings
Ni-Co, Ni-Fe, Ni-Fe-Co, Co-W, Co-Pt, Fe-Pt	Magnetic alloys
Cr-Mn, Cr-W, Cr-Mo, W-Fe	Heat-resistant alloys
Pd-Ni, Au-Ni, Au-Co	Coating replacing individual noble metals in electronics and jewelry
Pb-Ag, In-Pb, Pb-Cu, Ag-Sn	Antifriction alloys
Cu-Zn	Adhesion coatings
Ag-Sb, Ag-Pd, Au-Pd, Pd-Ni, Au-Ni, Au-Sb, Pd-In, Rh-In, **Fe-Cu**, Cu-Cr	Electric contact coatings, electrical device components, electrical connectors

These combinations of metals are found in many applications and this filed is still being developed due to the many new challenges and requirements as shown in Tab. 3. Electrochemically deposited alloys often feature properties and performance which are hard to obtain when the application of individual components is considered. Therefore, electroplating is a convenient way to introduce new properties and to functionalize the material surface.

6. Methodology

6.1. Materials and solutions

Electrodeposition was carried on the AISI 304 stainless steel (Fig. 10) plates (current collectors) with mass approximately 3.3 g. The chemical composition of the substrates is presented in Tab. 4.

Tab. 4. Chemical composition of AISI 304 stainless steel

Elements (%m/m)							
Cr	Ni	C	Mn	Si	P	S	Fe
18.0	10.0	0.08	2.0	1.0	0.045	0.03	68.845

Before electrodeposition, the substrates were prepared in order to create a uniform surface and to remove any existing grease and surface oxides. First, the stainless steel plates were polished with SiC paper with 500, 800 and 1000 grit. After polishing, the substrates were cleaned in ultrasonic cleaner in acetone solution, rinsed with distilled water and dried with compressed air. Once the substrates were dried, they were weighted.

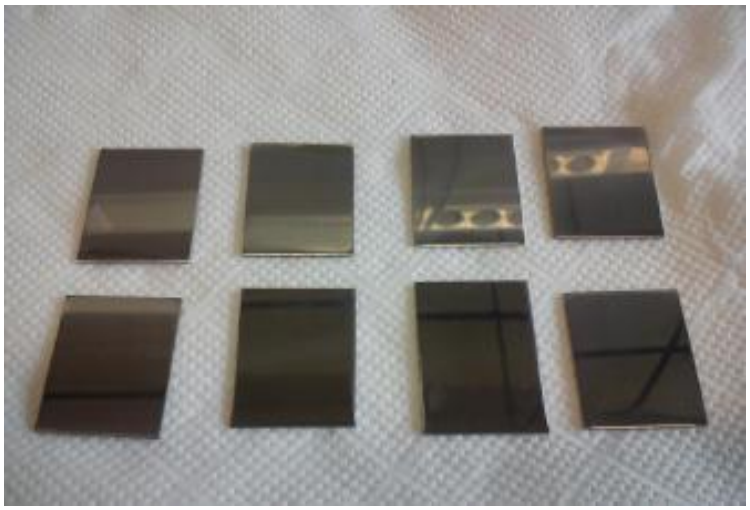

Fig. 10. Stainless steel substrates used for electrodeposition

The solutions used for electrodeposition were prepared from analytical grade chemicals and distilled water. A list of the solutions used in this work is presented in Tab. 5.

Tab. 5. Electrolytes used for electrodeposition.

	Solution composition
1.	0.5 M $FeCl_3$ + 1.5 M HCl + 0.01 M $CuSO_4$
2.	0.1 M $FeSO_4$ $7H_2O$ + 1.5 M H_2SO_4 + 0.01 M $CuSO_4$
3.	0.5 M $FeSO_4$ $7H_2O$ + 1.5 M H_2SO_4 + 0.01 M $CuSO_4$
4.	0.1 M $(NH_4)_2Fe(SO_4)_2 \cdot 6H_2O$ + 1.5 M H_2SO_4 + 0.01 M $CuSO_4$
5.	0.5 M $(NH_4)_2Fe(SO_4)_2 \cdot 6H_2O$ + 1.5 M H_2SO_4 + 0.01 M $CuSO_4$
6.	0.1 M $Fe(NO_3)_3$ + 1.5 M HNO_3 + 0.01 M $Cu(NO_3)_2 \cdot 3H_2O$
7.	0.25 M $FeSO_4$ + 0.25 M $NiSO_4$ + 0.01 M $CuSO_4$ + H_2SO_4
8.	0.5 M $FeSO_4$ + 1.5 M H_2SO_4 + 1 M HCl + 0.005 M $CuSO_4$
9.	0.5 M $FeSO_4$ + 1.5 M H_2SO_4 + 1 M HCl + 0.01 M $CuSO_4$

6.2. Electrochemical set-up

Electrodeposition of nanostructured metallic foams (NMFs) was performed on AISI 304 stainless steel substrates using a 2-electrode electrochemical cell connected to a DC power source. The setup used for electrodeposition is presented in Fig. 11 and consists of the following elements:

1) stainless steel plate of dimensions of 2.0 x 2.5 cm (working electrode).
2) lateral round hole that delimits and active area of 1.65 cm^2. An o-ring prevents electrolyte leakage
3) cylindrical electrochemical cell (7.0 cm of height and 5.0 cm width)
4) platinum counter electrode

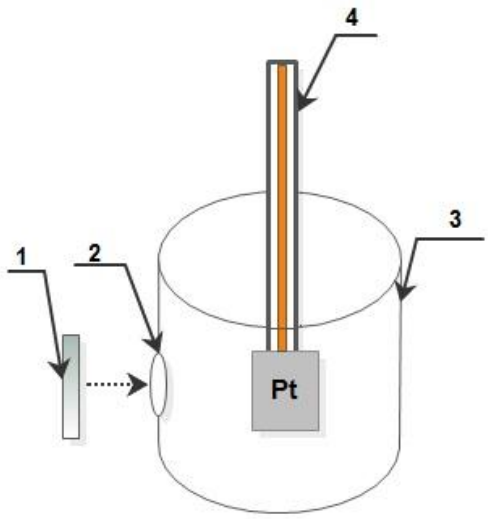

Fig. 11. Scheme of electrodeposition setup

The electrochemical testing of the NMFs was performed using the cell depicted in Fig. 11, but now the set up made use of a 3-electrode cell configuration connected to a Voltalab PGZ 100 potentiostat. The metallic foam was used as the working electrode, a platinum plate as counter

electrode and a saturated calomel electrode (SCE) as reference. All measurements were carried out in 1 M NaOH electrolyte at room temperature.

6.3. Electrodeposition parameters

In order to study the effect of electrodeposition parameters on the efficiency of the process and formation/structure of the NMFs, experiments were performed varying both applied current and deposition time. The data for electrodeposition parameters is presented in Tab. 6. Values regarding applied current are calculated basing on Eq. 4, where cross-section equaled 1.65 cm^2 in each case.

$$\text{current [A]} = \text{current density [A/cm}^2\text{]} \bullet \text{cross-section [cm}^2\text{]} \qquad \text{Eq. 4}$$

Tab. 6. Variation of applied current and time of electrodeposition.

Applied time [s]	Applied current [A]	Applied current density [A/cm^2]
30, 90, 120, 180	0.825	0.5
30, 90, 120, 180	1.650	1.0
30, 90, 120, 180	2.475	1.5
30, 90, 120, 180	3.000	1.8

After electrodeposition, substrates with deposited NMFs were rinsed gently with distilled water and dried with compressed air (at room temperature). Samples already prepared for the next tests are presented in Fig. 12.

Fig. 12. Substrates with deposited metals.

The substrates with deposited foams were weighted in order to obtain the net weight of the deposit.

6.4. Thermal conditioning

Heat treatment at various temperature was implemented in order to examine the role of temperature in the chemical and physical properties of the deposited foams. Thus, the selected samples were subjected to thermal conditioning at 150 °C or 250 °C in a Memmert oven. The residential time was set on 2 hours in the case of each temperature.

6.5. Characterization techniques

6.5.1. Scanning electron microscopy (SEM)

Scanning electron microscopy is a widely used tool for materials characterization. The technique is based on detection of signals originated from the interaction between a high energy electron beam and matter and provides information on surface topography, microstructure and chemical composition. The SEM image resolution, which is the ability to distinguish adjacent small features, is typically between 1 and 10 nm.

In a scanning electron microscope (Fig. 13), a focused high-energy electron beam scans the surface to be studied, and the signals derived from electron-sample interactions are analyzed [39]. SEM images are formed by signals resulting from the detection of secondary and/or backscattered electrons. Secondary electrons are weakly bonded electrons that are ejected from the sample due to its excitation by the primary electrons. They have low energy (< 50 eV) and as a result, they can only escape from the sample and be detected if they are generated near the surface, which makes them particularly informative on the topography and morphology of the sample. On the other hand, backscattered electrons originate from the backscattering of primary electrons by the nucleus of the sample atoms by elastic interactions (with small energy loss) and present much higher energy than the secondary electrons. The intensity of the backscattered electrons signal depends mainly on the mean atomic number of the sample atoms in the interaction volume, so they play an important role in illustrating contrasts in composition in the samples.

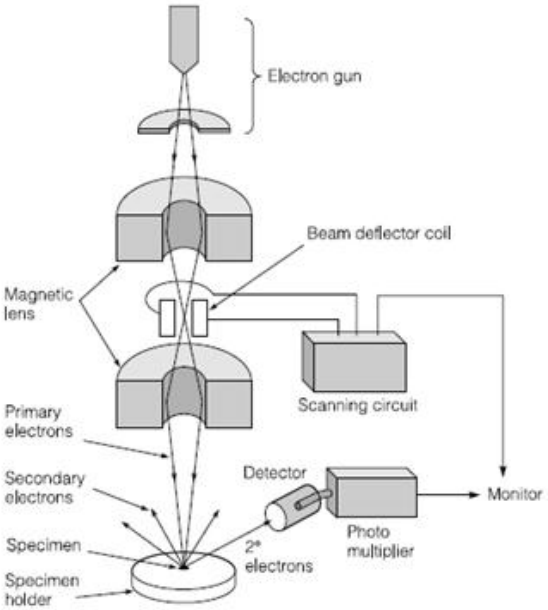

Fig. 13. Scheme of a scanning electron microscope.

Adapted from [40]

SEM may be applied in: *a)* generating high-resolution images of shapes and objects and to show variations in chemical composition, *b)* identifying phases based on qualitative chemical analysis, *c)* precise evaluation of very small features down to 10 nm, *d)* backscattered electron images may be used in order to obtain fast discrimination of phases in multiphase samples [41].

In this work, scanning electron micrographs were obtained with Hitachi S-2400 microscope using typically an acceleration voltage of 20 kV. This microscope provides an image resolution of 10 nm.

6.5.2. Energy dispersive X-ray spectroscopy

Energy dispersive X-ray spectrometry (EDS) is a chemical analysis technique that allows for determination of elemental composition of a sample by measuring the energy and intensity distribution of the X-ray signal generated by a focused electron beam interaction with the sample. EDS is typically coupled with scanning and transmission electron microscopes apparatus. This technique allows to determine the chemical composition of materials having a size of few microns as well as creating element composition maps. All elements from atomic number 4 to 92 can be detected. In EDS atoms within the sample are struck with an electron beam. This causes an excitement of electron from an inner atomic shell and its ejection from this shell, and thus, the electron hole is created. Such phenomenon is possible when electron from the beam has greater energy than inner shell electron binding energy. After the hole is created, it can be filled with an electron from an outer, higher-energy shell. The difference in energy between higher-energy shell and lower energy shell may be released in the form of an X-ray, or characteristic X-ray radiation. The second name, characteristic X-ray, is derived from the fact, that energy level of each electron is specific for every element and thus one is

able to obtain specific lines for measured samples. In order to obtain the specific lines, EDS systems consist of precise X-ray detector and software to collect and analyze energy spectrum. An EDS detector is mounted in the sample chamber of an electron microscope and contains crystal which absorbs the energy of approaching X-rays by ionization. The X-ray absorption converts the energy of radiation into electrical voltages of proportional magnitude and thus the electrical pulses correspond to the characteristic X-rays derived from the examined sample [39].

In this work, EDS analysis was performed using a Rontec standard EDS detector attached to the Hitachi S2400 SEM. EDS spectra analysis was performed by Wintools, comparing peak positions with a database for elemental identification. The characteristic energy lines of the elements usually observed in the samples studied in this work are compiled in Tab. 7.

Tab. 7. X-ray lines of elements typically found in Cu-Fe NMFs.

Element	X-ray line	
	K line (overlap)	**L line (overlap)**
Oxygen	0.523 (Cr, V)	
Copper	8.047	0.928
Iron	6.403 (Mn)	0.704 (F)

6.5.3. X-ray diffraction

X-ray diffraction is a non-destructive technique for materials characterization that allows for identification of phases present in a sample and to study their crystallographic structure, texture, residual stresses, etc. This method is commonly applied for studying crystal structures and atomic spacing (*d*). Crystals can be regarded as an arrangement of atoms in atomic planes spaced by a distance *d* apart. When there is the constructive interference from X-rays scattered by the atomic planes in a crystal, a diffraction peak is observed [39]. This condition occurs when Bragg´s law is obeyed:

$$n\lambda = 2d\sin\theta \qquad \text{Eq. 5}$$

This equation is very handy in identifying the structures of crystals since its derivation in early 1900's. The law relates the wavelength λ of the beam and the spacing *d* in the lattice. The incident angle is denoted by θ and *n* is any integer. In XRD, the sample and the detector rotate in order to obtain X-rays diffracted at specific angles. If Bragg's law is satisfied, constructive interference occurs and a diffraction peak is obtained (Fig. 14). A diffraction pattern is a graphical representation of the diffracted intensity versus the 2θ angle. For multiphase materials, the diffraction pattern is a weighted average of the individual diffraction patterns of each phase, proportionally to their volume fraction. Phase identification is usually performed by comparing the position of the three most intense peaks in the pattern with known patterns of pure substances referred in the JCPDS (Joint Committee on Powder Diffraction Standards) database.

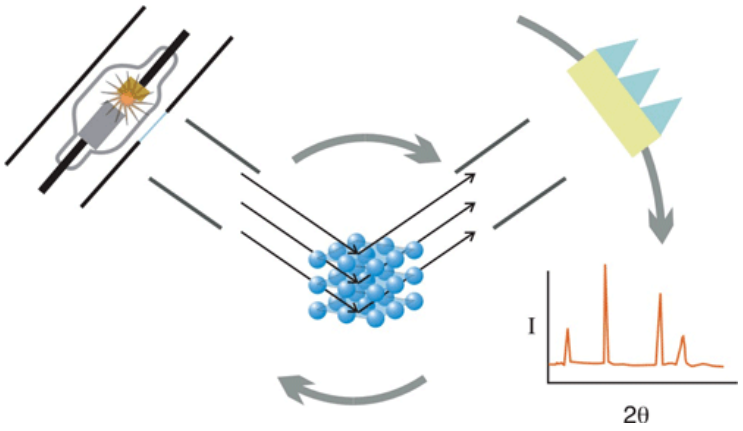

Fig. 14. XRD technique and conversion of d-spacings to diffraction pattern.

Adapted from [42]

In the present work, X-ray diffraction was performed using a Bruker D8 Advance diffractometer with a Bragg-Brentano geometry working with Cu radiation (0.154056 nm). Phase identification is performed by the Hanawalt method, comparing the position of the three most intense peaks in the pattern with known patterns of pure substances referred in the ICDD database.

6.5.4. Cyclic voltammetry

Cyclic voltammetry is an analytical electrochemical technique widely used to study electrode processes, that allows for a closer look into mechanisms of redox reactions and transport properties of a system. It is based on application of a variable potential to the working electrode while recording the electrical current response. This technique is ideal for a quick search of redox couples present in a system and evaluate the window of electrochemical stability [41]. As a result of a cyclic voltammetry measurement, the current at the working electrode is plotted versus the applied potential as shown in Fig. 15.

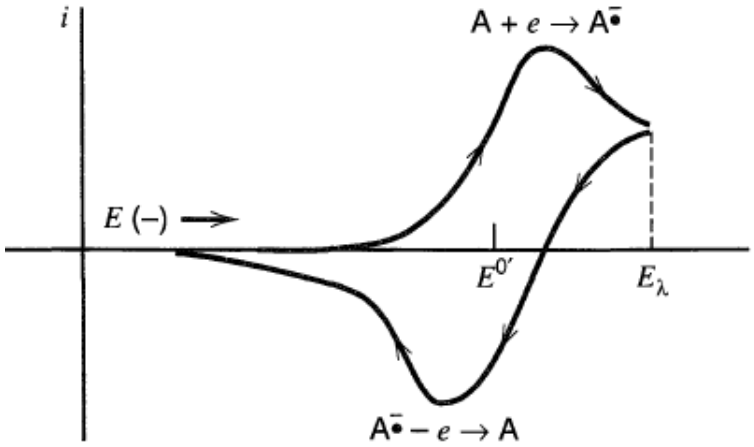

Fig. 15. Example of a cyclic voltammogram.

Adapted from [43]

In Fig. 15, the scan starts at the potential E(-) and is scanned in the positive direction up to a reverse potential (E_λ). When the standard potential of the redox reaction is reached, this reaction starts. When the potential of the working electrode is more positive than the standard potential of the redox reaction, the corresponding species may be oxidized and thus an anodic current is produced. When the return scan is carried out, the potential of the working electrode becomes more negative than the reduction potential of a redox couple and a cathodic current is created. As the applied potential becomes more negative, the concentration gradient at the electrode surface increases up to a value corresponding to the zero concentration of species “A” at the electrode surface. At the same time, species “A” diffuses from the solution bulk to the electrode surface. Both effects create a current peak that is not observed in steady-state conditions due to the very slow variation of the concentration gradient. The important parameters that can be extracted from the voltammogram are the cathodic and anodic peak currents and potentials. The relations between these parameters and the potential scan rate can be applied to assess the reversibility of the redox reaction.

In this work, cyclic voltammetry studies were performed using a 3-electrode electrochemical cell (Fig. 10) connected to a Voltalab PGZ 100 potentiostat where:

- the working electrode was the metallic foam to be tested deposited on a stainless steel substrate with an active area of 1 cm^2
- the counter electrode was a platinum spiral electrode
- a saturated calomel electrode (SCE) was used as reference

All measurements were carried out in 1 M NaOH electrolyte at room temperature. For voltammograms acquired for this work, the following parameters were used:

- Scan rate: 50 mV/s
- Maximum potential: 0 mV
- Minimum potential: -1500 mV
- Number of cycles: 10

The potential range selected for the experiments purposes satisfies the working potentials of pseudocapacitive-type materials basing on iron and copper [44].

6.5.5. Chronopotentiometry

Chronopotentiometry (galvanostatic charge-discharge) is useful measurement technique in the case of supercapacitors because it provides information about specific capacitance. In this technique, a constant current is applied between the counter and working electrodes while the potential of the working electrode is measured in relation to the reference electrode. The idea of the process is to

obtain the time in the set potential range in order to calculate capacitance of the electrodeposited foams.

Chronopotentiometry experiments were carried out in 1 M NaOH electrolyte at room temperature using the electrochemical set-up described for cyclic voltammetry. The input values which were set in order to execute the chronopotentiometry test were as follows:

- Applied current densities: 1 mA/cm^2 (charge) and -1 mA/cm^2 (discharge)
- Potential range: -1000 mV to 200 mV
- Number of cycles: 10

The specific capacitance of the metallic foams was calculated from charge-discharge data using the equation [1]:

$$C = \frac{i\Delta t}{m\Delta V} \qquad \text{Eq.6}$$

where *i* is the applied current density [mA/cm^2], Δt is the discharge time [s], *m* is the mass of active material [g] and ΔV is the potential window [V].

7. Results and discussion

7.1. Optimization of electrodeposition parameters: electrolyte solution, applied current and deposition time

Preliminary electrodeposition experiments were performed in a total of 9 electrolyte solutions, in order to select the most appropriate electrolyte for obtaining Cu-Fe metallic foams with high surface area. The results are summarized in Tab. 8.

Tab. 8. Results from electrodeposition experiments using different electrolyte solutions.

	Solution	Observations:
1.	0.5 M $FeCl_3$ + 1.5M HCl + 0.01 M $CuSO_4$	Deposition does not occur
2.	0.1 M $FeSO_4 \cdot 7H_2O$ + 1.5 M H_2SO_4 + 0.01 M $CuSO_4$	Deposition occurs, but Cu is mainly present in the foam
3.	0.5 M $FeSO_4 \cdot 7H_2O$ + 1.5 M H_2SO_4 + 0.01 M $CuSO_4$	Deposition occurs, but Cu is mainly present in the deposit while Fe amount is still insufficient
4.	0.1 M $(NH_4)_2Fe(SO_4)_2 \cdot 6H_2O$ + 1.5 M H_2SO_4 + 0.01 M $CuSO_4$	Deposition occurs, but molar concentration of ammonium iron (II) sulfate hexahydrate is too low to obtain promising foam structures
5.	**0.5 M $(NH_4)_2Fe(SO_4)_2 \cdot 6H_2O$ + 1.5 M H_2SO_4 + 0.01 M $CuSO_4$**	**Examined solution**
6.	0.1 M $Fe(NO_3)_3$ + 1.5 M HNO_3 + 0.01 M $Cu(NO_3)_2 \cdot 3H_2O$	Deposition does not occur
7.	0.25 M $FeSO_4$ + 0.25 M $NiSO_4$ + 0.01 M $CuSO_4$ + 1.5 M H_2SO_4	Deposition occurs , very low Fe content
8.	0.5 M $FeSO_4$ + 1.5 M H_2SO_4 + 1 M HCl + 0.005 M $CuSO_4$	Adding hydrochloric acid does not increase pores density, and the copper content of the foams increases
9.	0.5 M $FeSO_4$ + 1.5 M H_2SO_4 + 1 M HCl + 0.01 M $CuSO_4$	

As depicted in Tab. 8, electrodeposition from solutions 1 and 6 did not result in the formation of a deposit. In fact, after this procedure substrates were not covered at all or presented very unstable deposits that were not adherent to the substrate surface. Electrodeposition from solutions 2 and 3 resulted in the deposition of a foam-like structure, however, the amount of Fe in the deposited foams was very low (less than 10 at. %) even for solution 3 that has a higher $FeSO_4$ concentration. The deposits obtained from solution 7 did not present a 3D structure and the Fe content was quite low (< 5 at. %).

Solutions 4 and 5 both have the same chemical composition, but solution 5 has higher concentration of $(NH_4)_2Fe(SO_4)_2$. In these solutions, it was observed that increasing Fe concentration, resulted in a better developed 3D structure and, at the same time, in an increase of the Fe content in the deposit. Addition of HCl to the electrolyte, which is the case of solutions 8 and 9, did result in an

improvement of the foam-like structure, but the Fe concentration in the deposits decreased to less than 10 at. %. Fig. 16. depicts SEM images of samples electrodeposited from rejected solutions.

Taking these results into consideration, solution 5 was chosen as electrolyte for subsequent studies. An overview of the electrodeposition experiments performed by varying the applied current and deposition time is presented in Tab. 9.

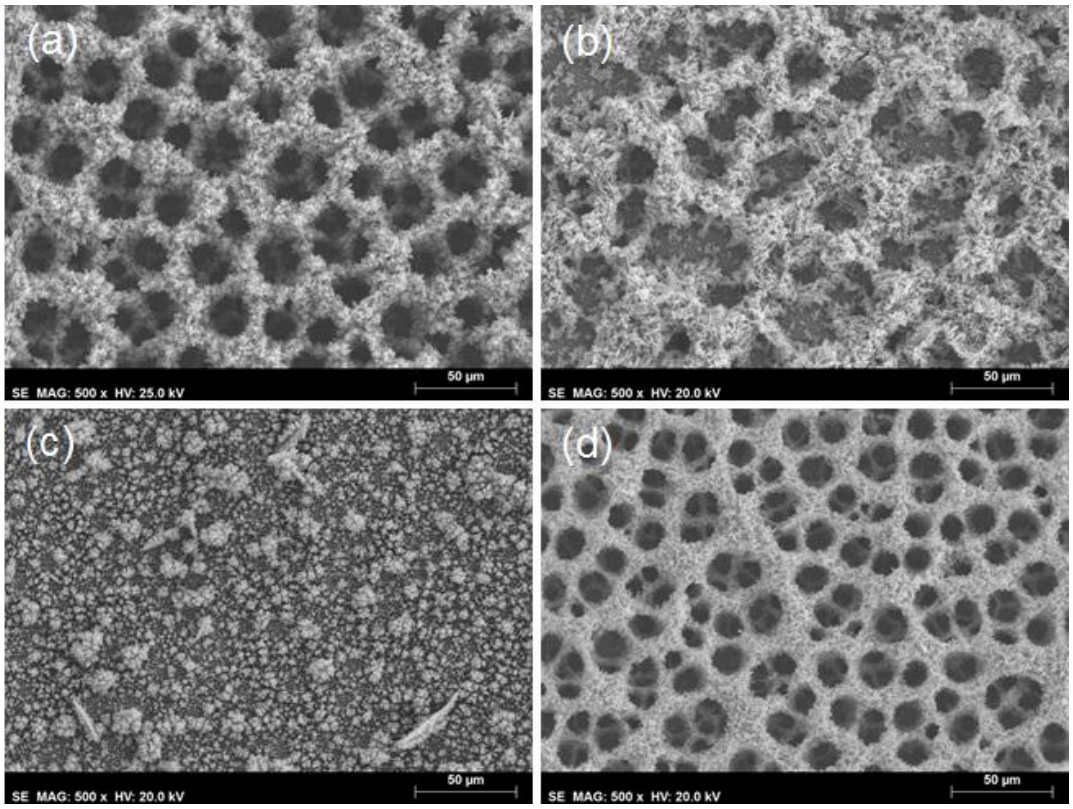

Fig. 16. SEM images (of films electrodeposited at 3A for 180 s from (a) - solution no. 2, (b) - solution no. 3, (c) - solution no. 7, (d) - solution no. 9.

Tab. 9. Samples obtained from electrolyte 5

	Deposition time [s]	Current [A]	Index
1.	90	0.825	90s_0.825A
2.	90	1.65	90s_1.65A
3.	90	2.475	90s_2.475A
4.	90	3.00	90s_3A
5.	180	0.825	180s_0.825A
6.	180	1.65	180s_1.65A
7.	180	2.475	180s_2.475A
8.	180	3.00	180s_3A

Electrodeposition at 0.825 and 1.65 A for 90 s resulted in smooth films with randomly distributed dendritic particles on the surface (Fig. 17). Increasing the deposition time to 180 s lead to increase of both number and size of particles at the surface but failed to produce a continuous 3D structure.

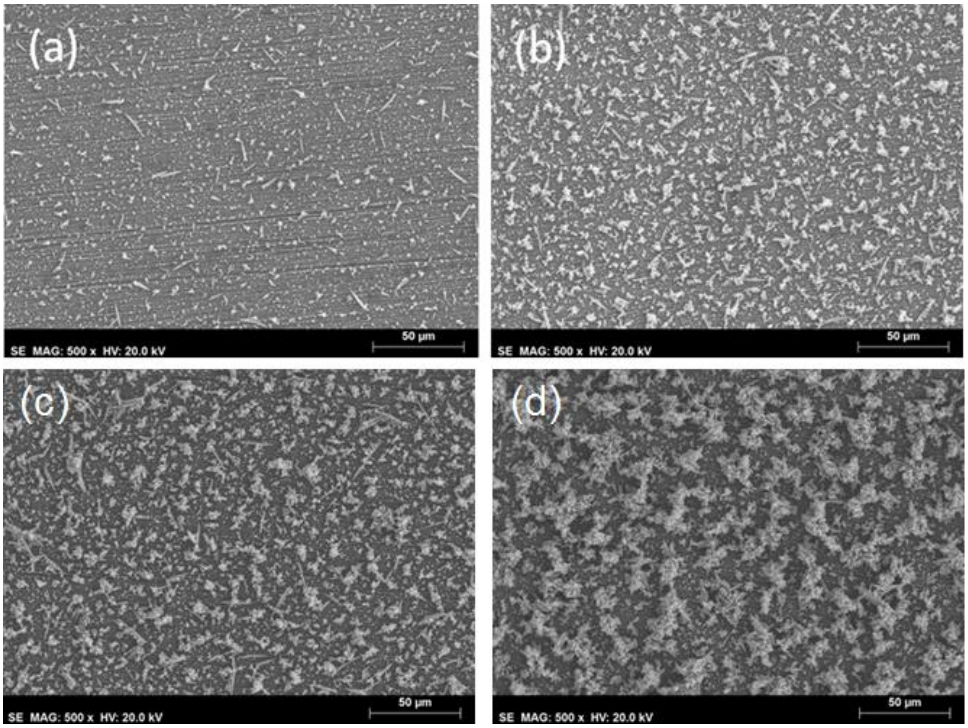

Fig. 17. Fig. 17. SEM images of films electrodeposited from solution 5 at 0.825 A and 90 s (a), 1.65 A and 90 s (b), 0.825 A and 180 s (c) and 1.65 A and 180 s (d).

Resulting samples 1, 2, 5, 6 and 7 were rejected from further studies due to poor deposit content on the surface and insufficient Fe content (less than 20 %). Three samples having the highest amount of Fe (on the basis of EDS analysis) were chosen for full characterization, as presented in Tab.10.

Tab. 10. Identification of raw samples selected for tests.

	Deposition time [s]	Current [A]	Index
1.	90	2.475	**90s_2.475A**
2.	90	3	**90s_3A**
3.	180	3	**180s_3A**

Selected samples were subjected to heat treatment at temperatures of 150 and 250 ^{o}C in order to determine if their performance was improved. Heat treated samples along with corresponding indices are presented in Tab. 11.

Tab. 11. Description of heat treated samples.

Raw sample index	Temperature [°C]	Index of heat treated sample
90s_2.475A	150	**90s_2.475A_150C**
	250	**90s_2.475A_250C**
90s_3A	150	**90s_3A_150C**
	250	**90s_3A_250C**
180s_3A	150	**180s_3A_150C**
	250	**180s_3A_250C**

7.2. Morphology

7.2.1. Morphological characterization of the raw samples

Selected samples were analyzed by SEM in order to characterize the deposited structures. As can be noticed from the images below (Fig. 18 to 20), increasing time of deposition as well as applied current can significantly change the 3D foams.

Fig. 18. presents SEM images of deposits obtained by applying a current of 2.475 A for 90 s (90s_2.475A). As it may be seen, dispersed dendrite structures have been formed over a continuous thin film composed of angular grains. Furthermore, spacing between the dendritic structures is approximately 20 μm (see squares in Fig. 18c), and may be related to the formation of hydrogen bubbles during deposition.

In the films deposited at a higher current (3 A) for 90 s (Fig. 19), the density of dendritic structures formed increases and a network of dendritic walls is formed. The dendrites do not present any preferential growth direction (in relation to the substrate), being randomly oriented. As indicated in Fig.19c (white squares), the distances between the dendritic structures are slightly smaller than in sample 90s_2.475A, ranging from 15 to 20 μm.

Films prepared at 3 A for 180 s are shown in Fig. 20. The continuous thin film formed at the substrate's interface is still visible, but, and contrarily to the previous samples, a 3D honeycomb-like dendritic structure is also observed, similarly to other studies on copper electrodeposition [32]. The formation of this structure is related to hydrogen bubbles forming at the active sites during the electrodeposition process. Due to the high cathodic current applied, deposition of Cu and Fe occurs simultaneously with intense hydrogen evolution, which is easily seen during deposition experiments. Metal deposition occurs preferentially in the space between hydrogen bubbles, forming metal grains. H_2 bubbles grow (or coalesce) with time and eventually detach from the substrate, creating regular shaped pores in the growing deposit. Furthermore, hydrogen bubbles will also evolve at different locations and depths in the growing metallic foam, leading to a wide size distribution of surface pores.

As can be seen in Figs. 18 to 20, the deposition time plays an important role regarding the amount of film deposited. When the deposition time was 90 s, hydrogen bubbles evolve during

deposition, but in the moment they get detached from the surface, there is not enough time for the growth of metallic agglomerates to occur around the evolving bubbles and create a 3D deposit. The irregularities of deposited foams in case of samples 90s_2.475A and 90s_3A may result from short deposition time.

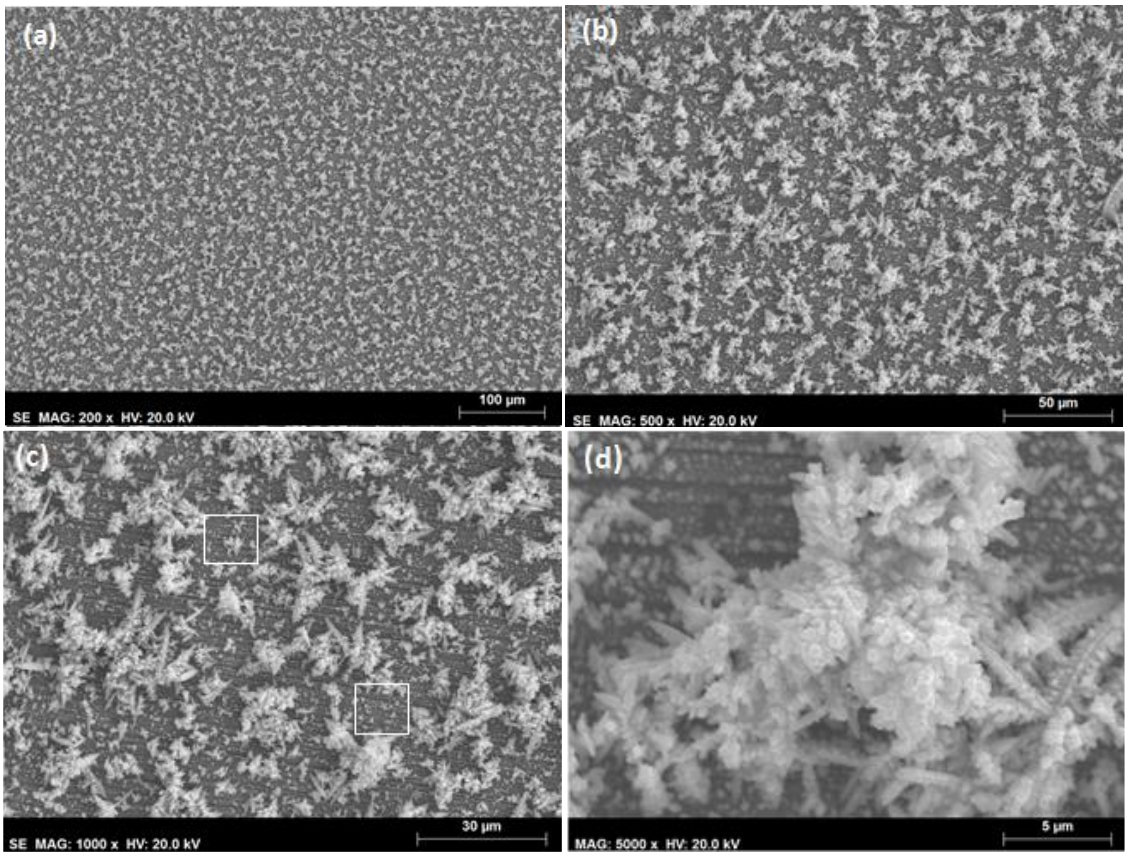

Fig. 18. SEM images of Cu-Fe deposits for sample 90s_2.475A at different magnifications: a) 200x, b) 500x, c) 1000x, d) 5000x.

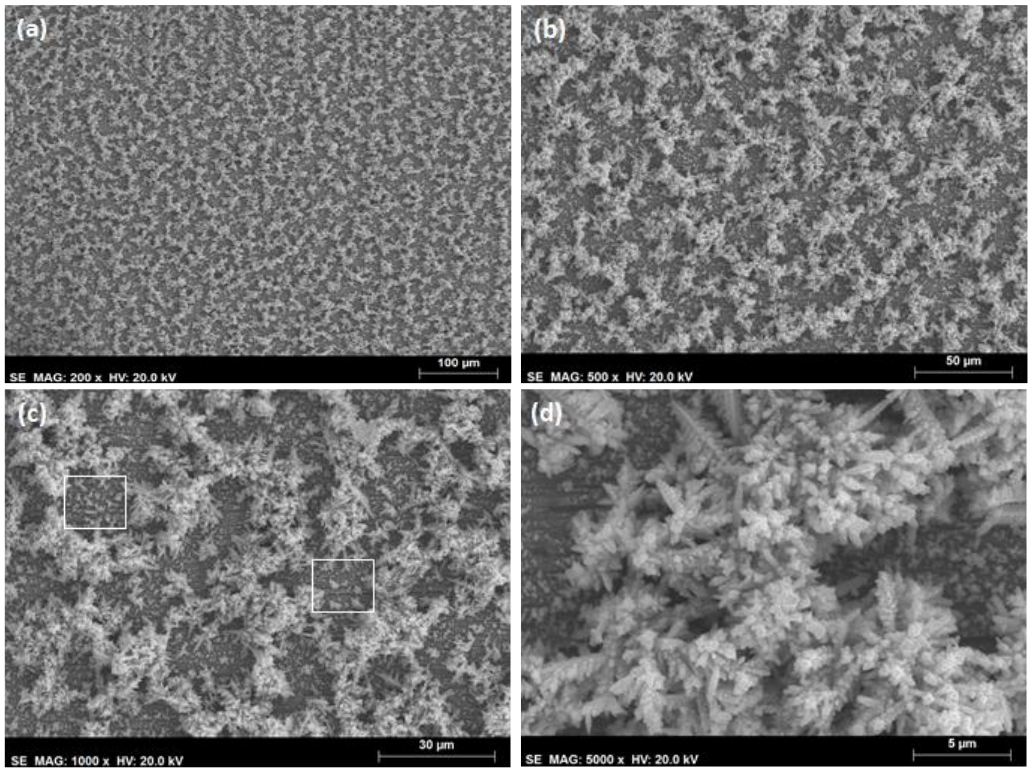

Fig. 19. SEM images of Cu-Fe deposits for sample 90s_3A at different magnifications: a) 200x, b) 500x, c) 1000x, d) 5000x.

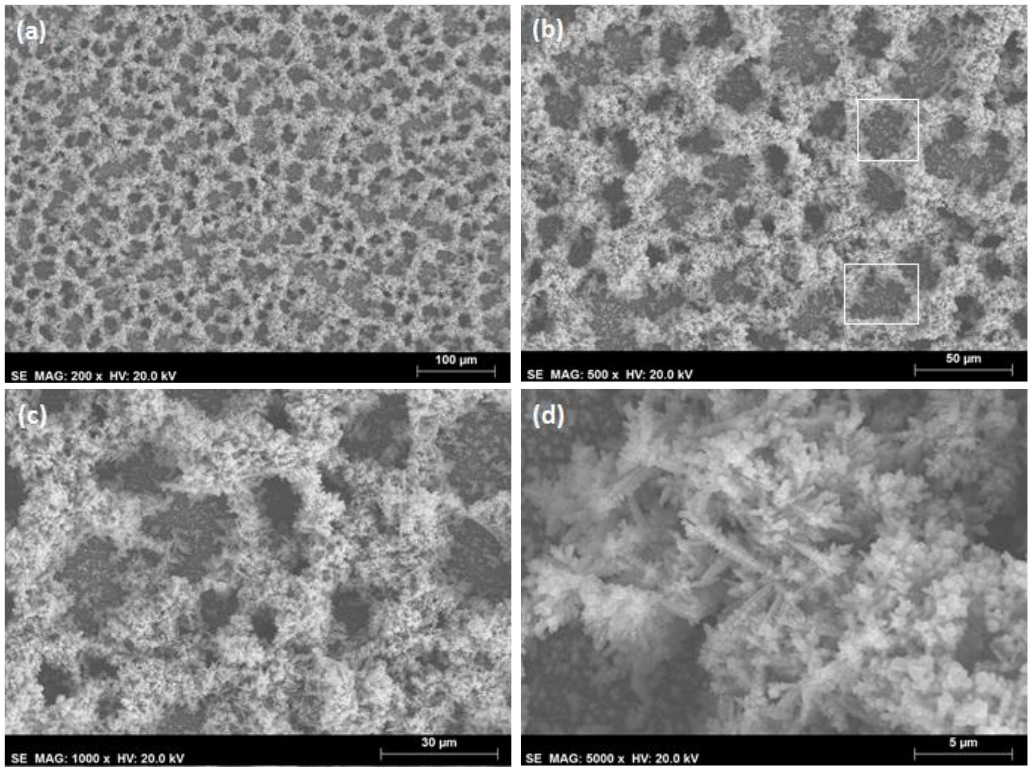

Fig. 20. SEM images of Cu-Fe deposits for sample 180s_3A at different magnifications: a) 200x, b) 500x, c) 1000x, d) 5000x.

As can be seen in Fig. 20, there are different types of holes/craters in the deposits, marked with white squares in Fig. 20b. One type (upper square) presents a nearly circular shape and originates from the formation of hydrogen bubbles at the substrate around which the metal will deposit. A second type of craters (lower square) presents an irregular shape and their formation may be explained by the nucleation and growth of adjacent metal grains that will join the closely formed agglomerates and thus form irregular holes [32].

7.2.2. Morphological characterization of the heat treated samples

As it was already mentioned in chapter 6.4, metallic foams obtained by electrodeposition were subject of heat treatment at 150 and 250 °C for 2 hours. SEM images of the samples before and after treatment were obtained to find out if there are any changes in the morphology of the foams due to the heat treatment (Figs. 21 to 23).

As can be seen, SEM images at magnification of 1000x do not differ in a significant way. The lengths of the spots covered with Cu-Fe grains remain the same comparing to the raw sample. The structure was not broken and remains nearly unaltered after heat treatment. However, higher magnification images (5000x) show that the grain size of the deposited film increases with the heat treatment temperature (Fig. 21 d, e and 21 f). This result is attributed to the oxidation process.

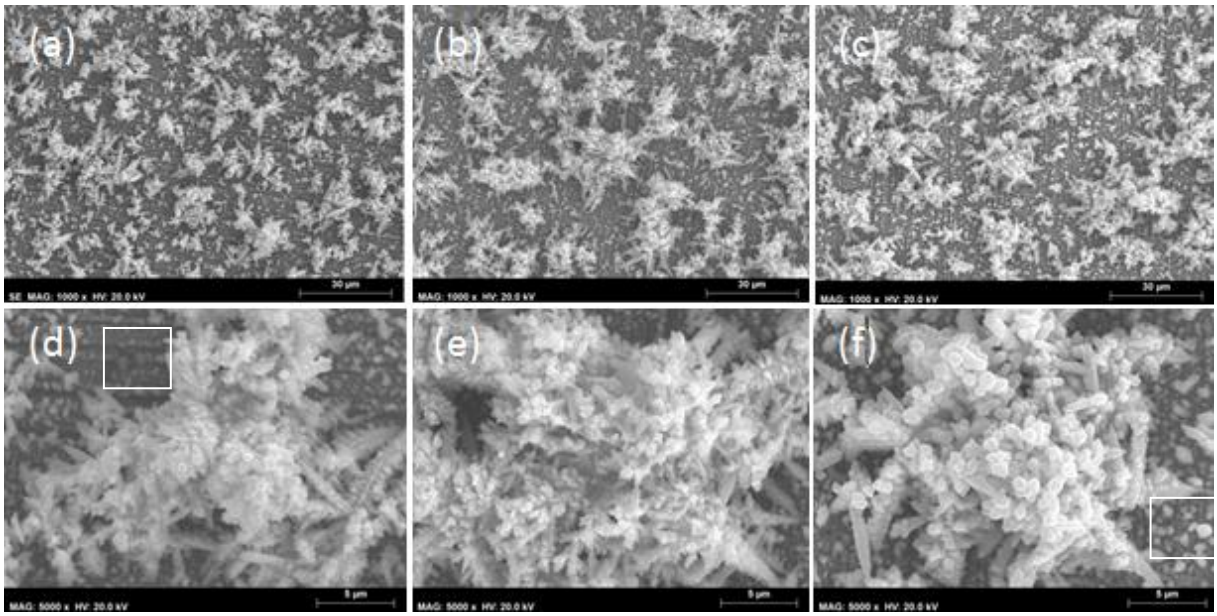

Fig. 21. SEM images of metallic foam deposited at 2.475 A for 90 s (a, d) as is and after heat treatment at (b, e) 150 ºC and (c, f) 250 ºC.

White ellipse in Fig. 22c points out that the increase of grain size seems to occurs also in the smooth film formed at the interface with the substrate.

Heat treatment of samples deposited at 3 A for 90 s resulted in similar morphology evolution (Fig. 22), with the grain size increasing with the temperature of the treatment.

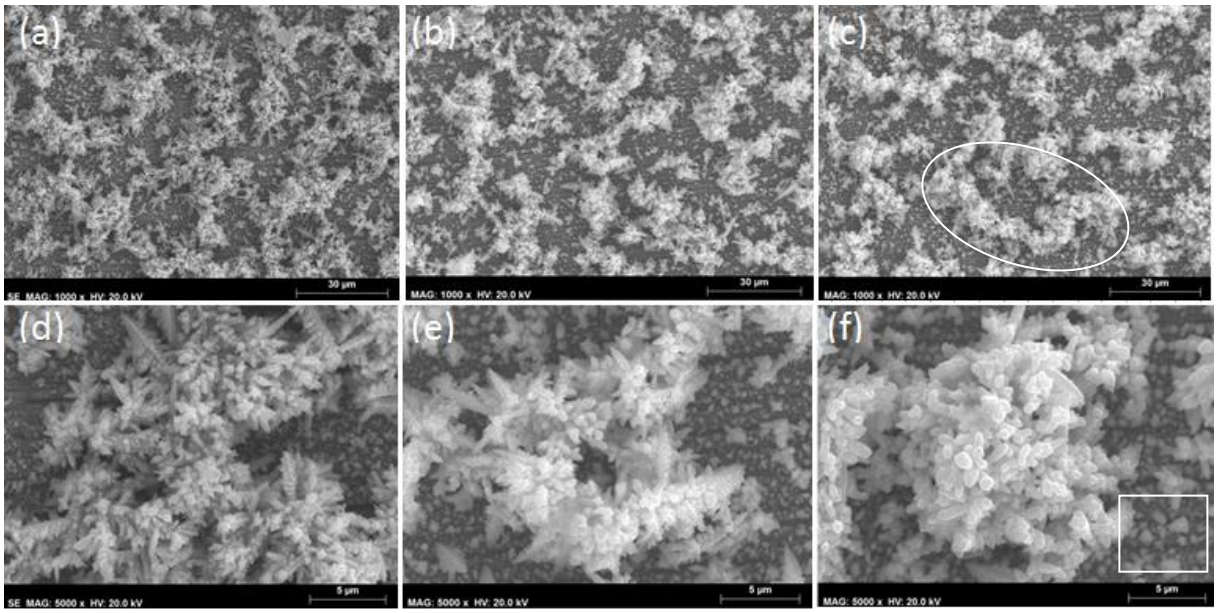

Fig. 22. SEM images of metallic foam deposited at 3 A for 90 s (a, d) as it is and after heat treatment at (b, e) 150 ºC and (c, f) 250 ºC.

SEM images of films deposited at 3 A for 180 s before and after heat treatment are presented in Fig. 23. As in other samples, the 3D structure is kept after the heat treatment. High magnification images show that the branches of the dendrites become coarser after heat treatment and have dimensions of approximately 1 μm after heat treatment at 250 °C (white circles in Fig. 23i).

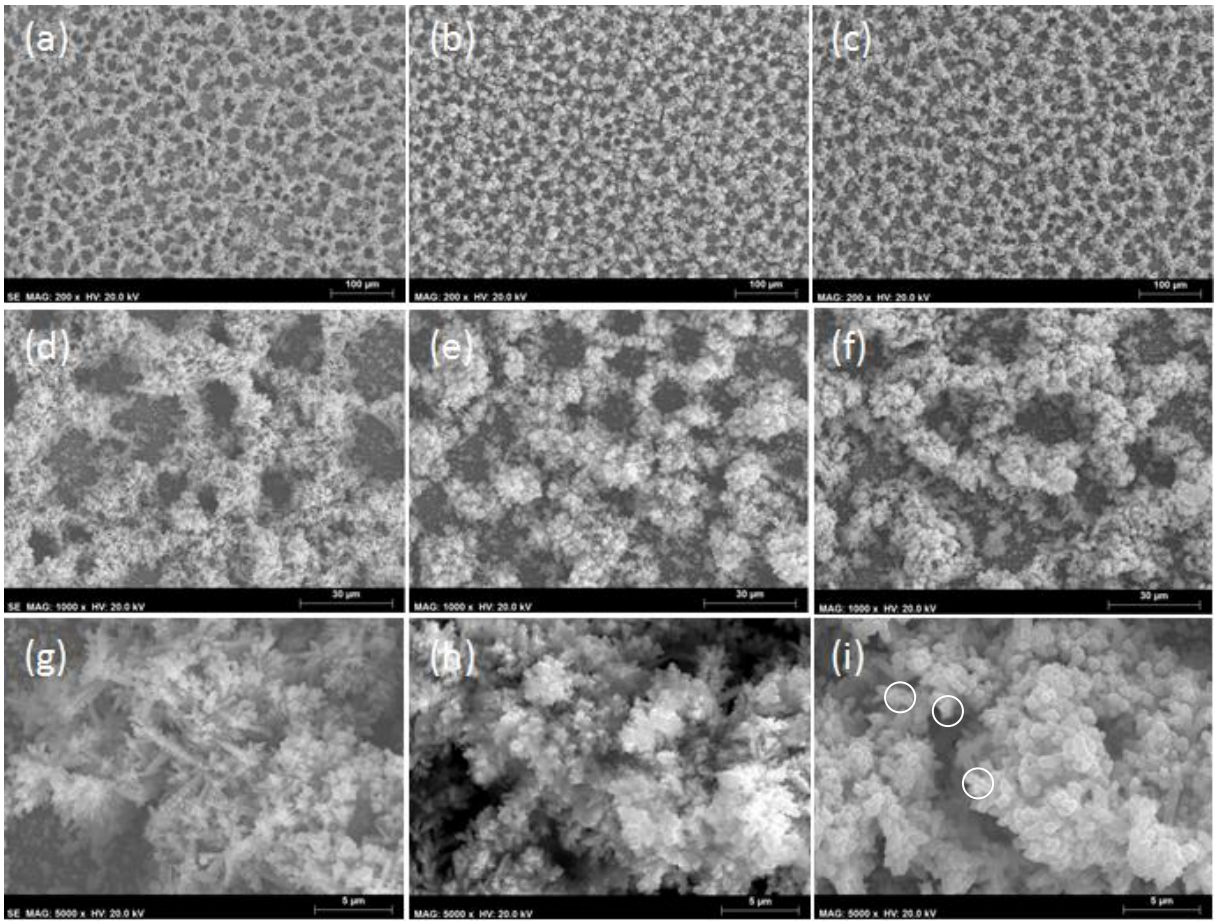

Fig. 23. SEM images of metallic foam deposited at 3 A for 180 s (a, d, g) as it is and after heat treatment at (b, e, h) 150 °C and (c, f, i) 250 °C.

7.2.3. Chemical composition of the metallic foams

Chemical composition of the electrodeposited foams was studied by EDS and, as expected, the main elements detected were copper and iron. A typical EDS spectrum of the metallic foam obtained at 2.475 A for 90 s is presented in Fig. 24.

Dependence of the average Cu and Fe atomic percentages in the films on the deposition conditions is shown in Fig. 25. Iron content of the metallic foams tends to increase with the applied current density and decreases with deposition time. Increased current of electrodeposition process resulted in increasing Fe content in samples obtained after 90 seconds (from 23 % to 36 %). In the case of sample 180s_3A, improved time resulted in identical proportions of metals as found in sample 90s_2.475A. It means that in order to obtain more iron in the foam structure it is necessary to limit the deposition time due to more intense copper deposition after a period of 90 seconds.

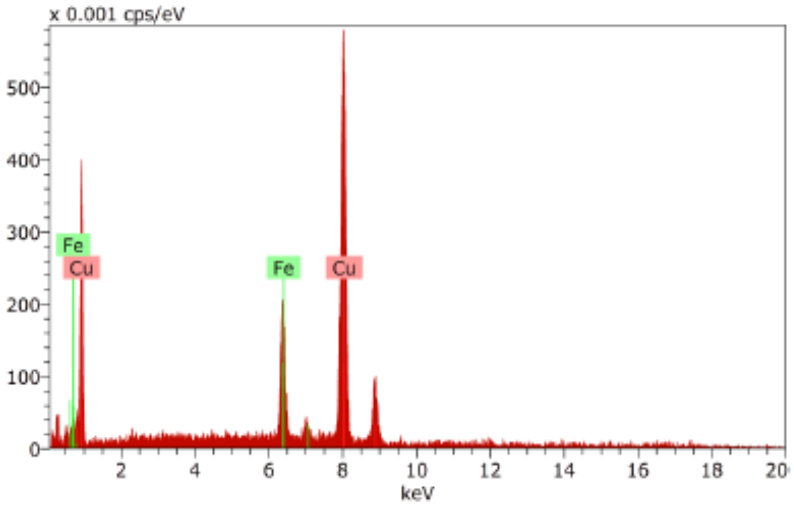

Fig. 24. EDS spectrum of metallic foam obtained at 2.475 A for 90 s.

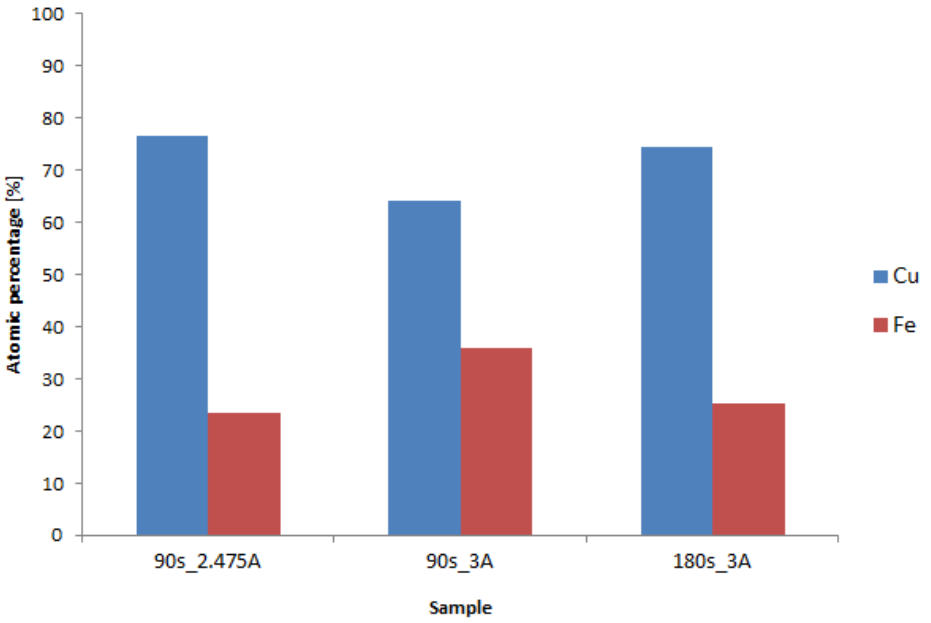

Fig. 25. Variation of Cu and Fe content of the foams with the deposition parameters.

It should also be noted that the copper content in the foams is much higher than that in the deposition electrolyte. In solution, copper represents only 2 at. % of the metallic ions but it reaches up to almost 80 at. % in metallic foams. The standard reduction potential of copper (+0.337 V) is about 0.7 V less negative (more noble) than that of iron (-0.41 V). Hence, during electrodeposition of Cu-Fe foams, Cu, being the most noble metal, deposits preferentially to Fe, explaining the reason why the content of Cu in the deposited foam is higher than in solution.

EDS analysis was also performed in the same three samples after heat treatment (at 150 and 250 °C). As expected, the only difference is that heat-treated samples present oxygen in their chemical composition with atomic percentage ranges from approximately 10 % (at 150 ºC) up to 28 % (at 250 ºC).

7.2.4. Dependency of deposited mass on current density and deposition time

As expected, the mass of deposits increases with the deposition time and the applied current. This behavior is presented in Fig. 26. In order to present increasing character, the additional samples are included i.e. 0.825 A and 1.65 A for 90s as well as 0.825 A, 1.65 A and 2.475 A for 180s. The obtained results for deposit mass indicate that current which is applied plays significant role in electrodeposition process in this study. The time which is used is also a factor that improves the mass of deposited foams.

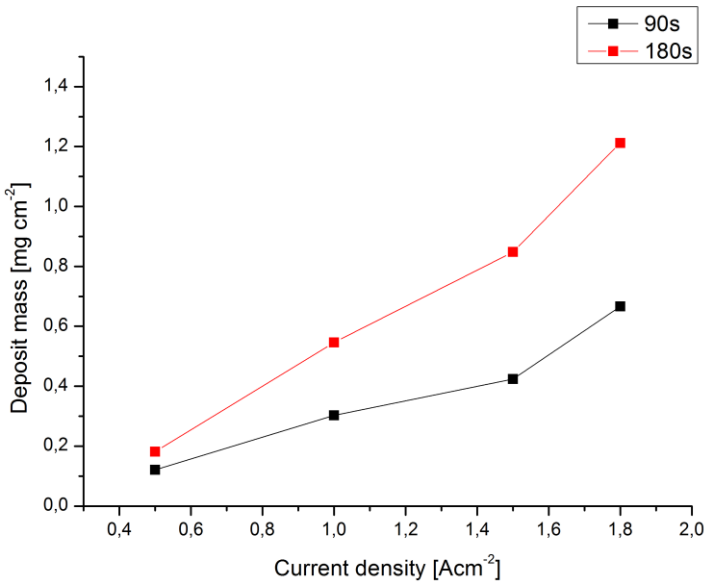

Fig. 26. Relationship between deposit mass and applied current density.

7.3. XRD analysis

XRD analysis was carried out on Cu-Fe foams deposited at 3A for 180 s before (sample 180s_3A) and after heat treatment at 150 ºC (180s_3A_150C) and 250 ºC (180s_3A_250C). The resulting diffractograms are presented in Fig. 27.

The diffractogram of sample 180s_3A contains four peaks. The peaks at 43.4°, 50.5° and 74.2° correspond to (111), (200) and (220) planes of face-centered cubic copper (ICDD 01-070-3039), respectively. Peaks related to an iron phase were identified at 44.6° and 82.3° which are attributed to (110) and (211) planes of body-centered cubic iron (ICDD 03-065-4899). This result is also in agreement with other studies in the literature [45].

After heat treatment at 150 °C, the diffractogram does not present significant changes (Fig. 27). After heat treatment at 250 °C a new peak is observed at 36.4º which corresponds to (111) plane of Cu_2O (ICDD 077-0199). These results indicate that the heat treatments lead to the partial

oxidation of the Cu-Fe films and to the formation of Cu_2O, in agreement with the EDS results that indicated a high oxygen content. Peaks related to the formation of iron oxides could not be identified at the diffractograms, probably due to the small amount of that phase.

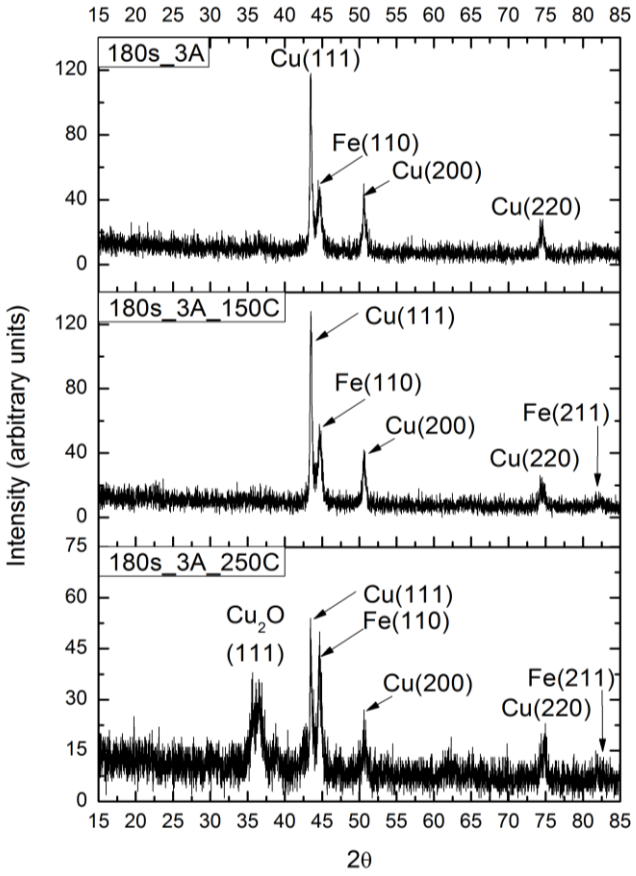

Fig. 27. Diffractograms of Cu-Fe foams obtained at 3A current and 180s before and after heat treatment.

7.4. Electrochemical characterization

7.4.1. Cyclic voltammetry results

Cyclic voltammetry tests of Cu-Fe foams were carried out in 1 M NaOH electrolyte within a potential window between -1.5 and 0 V. Representative cyclic voltammograms of Cu-Fe foams (Figs. 28 to 30) are not square-shaped as those of materials that exhibit an electric double layer charge storage mechanism [1].

Electrochemical behavior of the tested samples is very similar. In general, three reduction peaks and three corresponding oxidation peaks can be identified (Fig. 28) and related to the following reactions [46, 47, 48]:

$$Ox1/Red1: Fe + 2OH^- \leftrightarrow Fe(OH)_2 + 2e^- \quad \text{Eq. 7}$$

$$Ox2/Red2: 2Cu + 2OH^- \leftrightarrow Cu_2O + H_2O + 2e^- \quad \text{Eq. 8}$$

$$Ox3/Red3: Cu_2O + 2OH^- + H_2O \leftrightarrow 2Cu(OH)_2 + 2e^- \quad \text{Eq. 9}$$

These reactions result in the pseudocapacitive behavior of the deposited foams, since they induce the transition between different oxidation states. Moreover, existence of peaks corresponding to Fe and Cu in the cyclic voltammograms is related to co-deposition of these metals on the substrate.

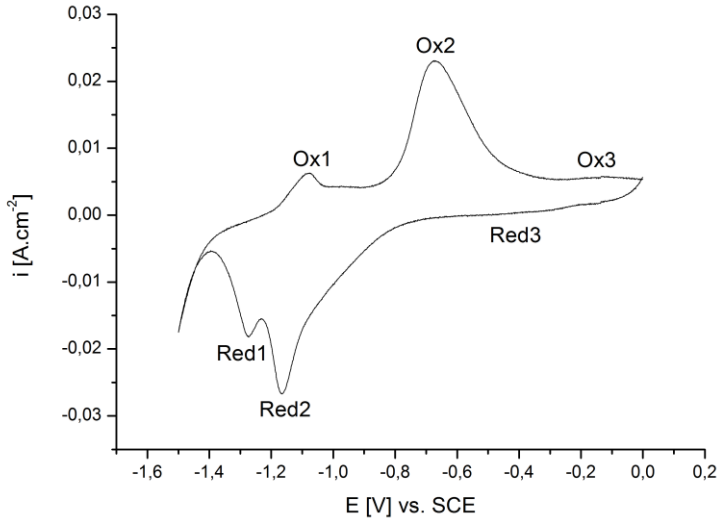

Fig. 28. Typical peaks occurring in the voltammograms. Sample 90s_2.475A_150C. Scan rate 50 mV/s.

Comparison of cyclic voltammograms of raw samples is presented in Fig. 29. Along with increasing current and time of electrodeposition specific area increases. Plot corresponding to the 180s_3A sample contains higher peaks related to Eq. 9. The peaks observed in Fig. 29 are slightly shifted to negative values when compared to the reduction and oxidation potentials of pure copper and iron found in other studies [44, 46] (Tab. 12). This can be related to the presence of both metals in the foam.

Tab. 12. Peak potentials for Fe and Cu according literature.
Adapted from [44, 46]

Reaction	Oxidation potential [V] vs. SCE	Reduction potential [V] vs. SCE
$Fe + 2OH^- \leftrightarrow Fe(OH)_2 + 2e^-$	-0.7	-1.2
$2Cu + 2OH^- \leftrightarrow Cu_2O + H_2O + 2e^-$	-0.4	-0.9
$Cu_2O + 2OH^- + H_2O \leftrightarrow 2Cu(OH)_2 + 2e^-$	-0.2	-0.35

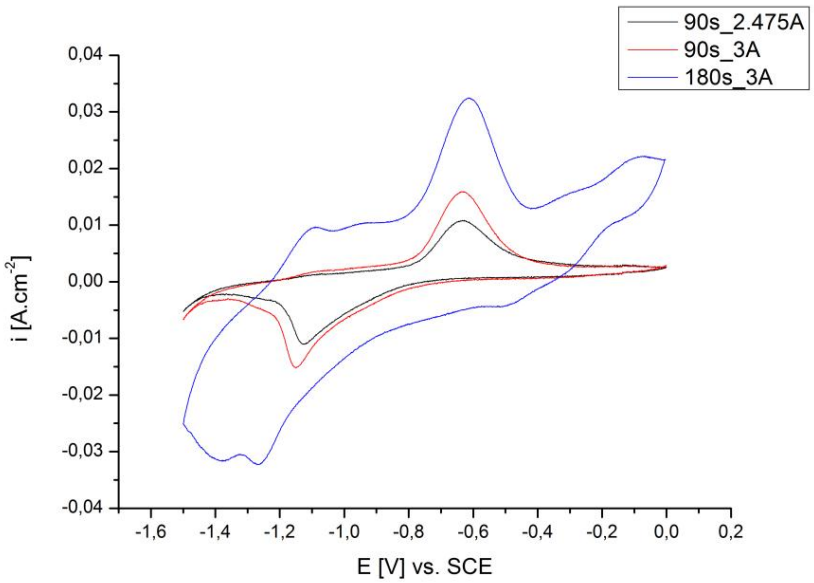

Fig. 29. Cyclic voltammograms of Cu-Fe foams deposited in different conditions in 1 M NaOH. Scan rate 50 mV/s.

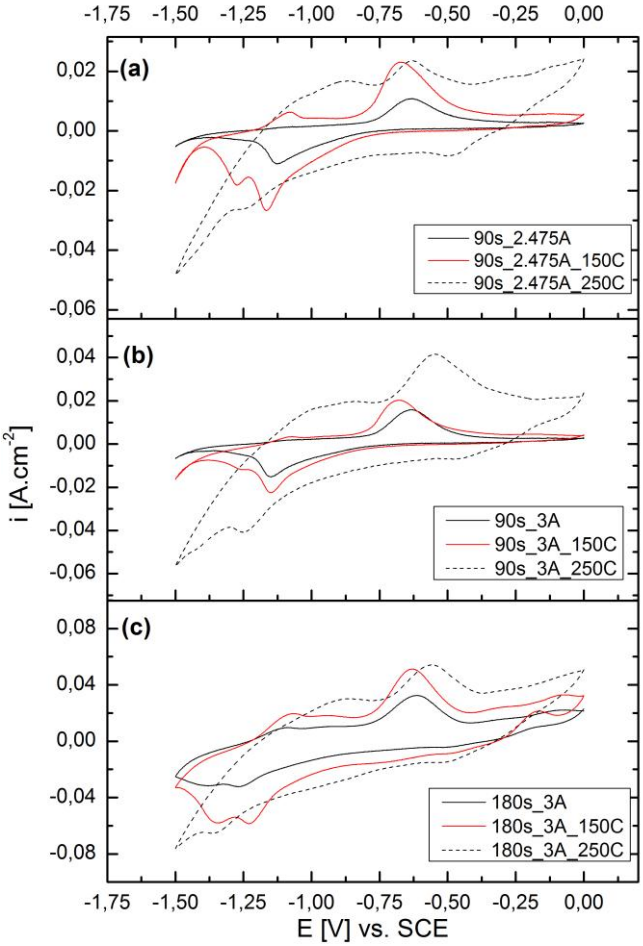

Fig. 30. Cyclic voltammograms of Cu-Fe foams before and after heat treatment in 1 M NaOH. Scan rate 50 mV/s.

Fig. 30 depicts cyclic voltammograms from all raw samples and their heat treated correspondents. Cyclic voltammograms of heat treated samples show larger redox peaks corresponding to Eq. 7 and Eq. 9. This is attributed to the enhancement of these redox reactions due to the oxidation of the foams during the heat treatment, as described in chapters 7.2.3 and 7.3

7.4.2. Charge-discharge curves

Chronopotentiometric tests (charge-discharge curves) were conducted in 1 M NaOH solution. The typical shape of charge-discharge curves, for sample 90s_2.475A is presented in Fig. 31.

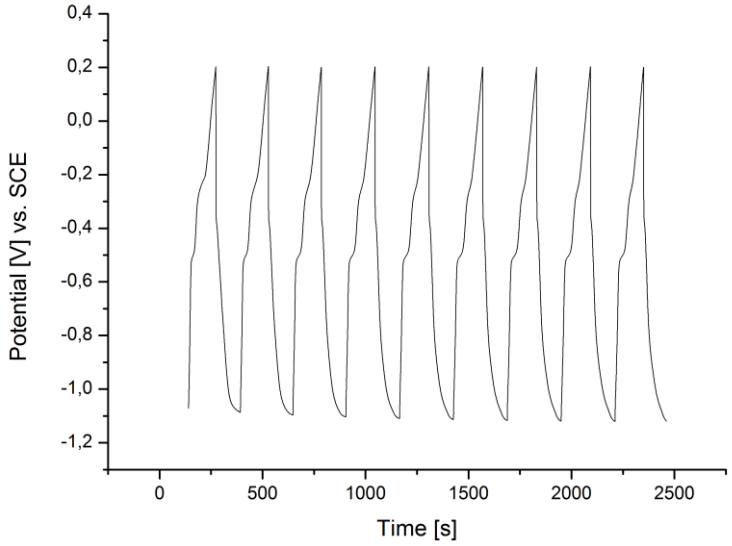

Fig. 31. Typical charge-discharge curves obtained for sample 90s_2.475A. Applied charge and discharge current is equal +1 mA/cm^2 and -1 mA/cm^2, respectively.

Analysis of second discharge curve allows for specific capacitance calculations. Comparison of discharge curves of raw samples 90s_2.475A, 90s_3A and 180s_3A is presented in Fig. 32 . As can be seen, samples obtained in time of 90 second deposition are able to reach set potential range (from -1 V to +0.2V) whereas sample 180s_3A reaches potential window of -0.25V and -0.9V.

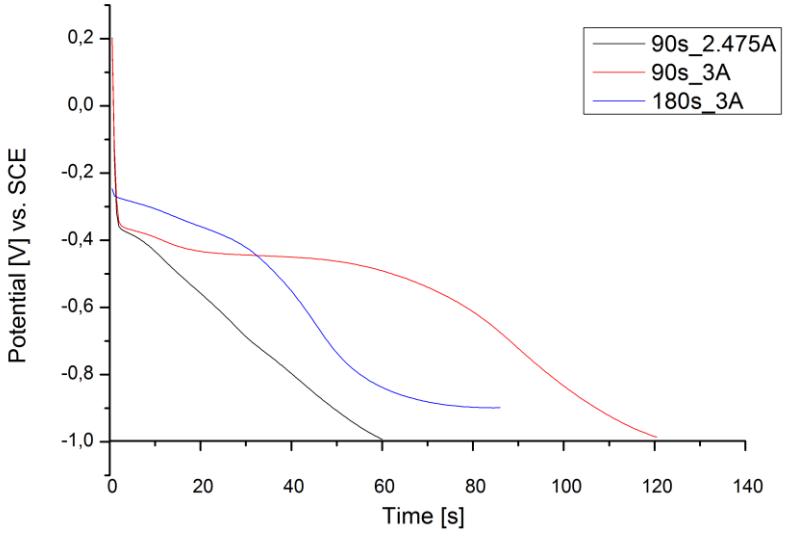

Fig. 32. Raw samples discharge curves comparison. Discharge current is equal -1 mA/cm^2.

Using the data from the discharge curves and applying Eq. 6 it is possible to calculate specific capacitance of the deposits. The results are presented in Tab. 13.

Tab. 13. Values for specific capacitance obtained from the charge discharge curves.

Sample	Current [A]	Discharge time [s]	Potential window [V]	Mass of deposit [g]	Specific capacitance C [Fg^{-1}]
90s_2.475A	0.001	60	1.2	0.0004	137.50
90s_3A	0.001	120.5	1.2	0.0006	165.69
180s_3A	0.001	86	0.65	0.0012	114.90
Results regarding sample 90s_2.475A after heat treatment at 150 °C and 250 °C					
90s_2.475A_150C	0.001	89.5	1.2	0.0004	205.10
90s_2.475A_250C	0.001	77	1.2	0.0004	176.46

From the above table it may be seen, that despite higher deposit mass, sample 180s_3A presents a lower value of discharge capacity than the sample obtained with the same current but with lower deposition time (90s_3A). Furthermore, the potential window reached by this sample equals 0.65V and the charge-discharge curves do not have the sharp peak as observed for the sample 90s_2.475A. Based on these results, focus was placed on sample 90s_2.475A and its heat treated correspondents (90s_2.475A_150C and 90s_2.475A_250C) – Tab. 13.

Fig. 33 presents the second charge/discharge curves of the raw 90s_2.475A and heat treated samples. This figure confirms the values obtained in Tab. 13, where sample subjected to heat treatment at 250 °C was able to perform better than the raw sample. Sample treated at 150 °C demonstrates the best performance in terms of time of charge-discharge and related specific capacitance (205 Fg^{-1}).

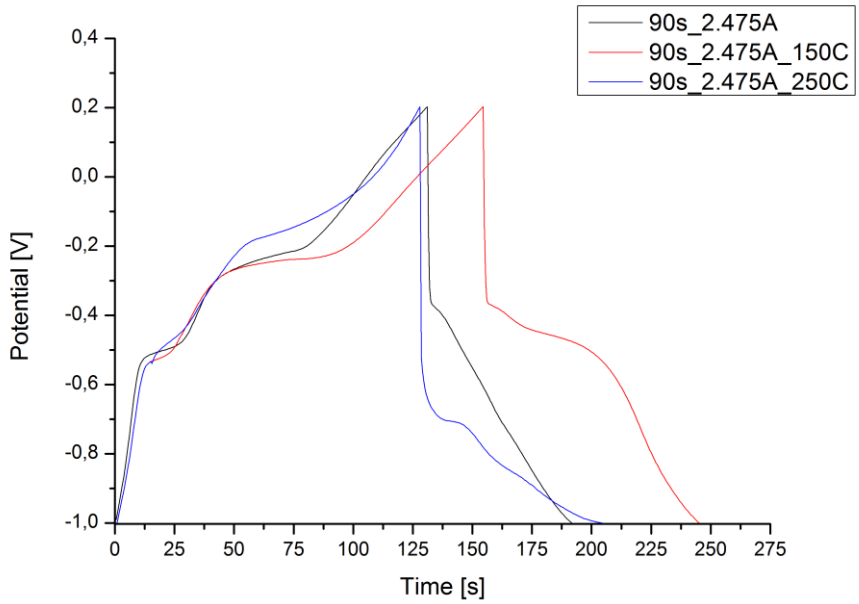

Fig. 33. Comparison of charge-discharge curves of raw and heat treated samples obtained in 90s and 2.475A current.

7.4.3. Capacitance dependency on the number of cycles

Charge-discharge longtime performance measurements were carried out in order to determine the dependence of the capacitance on the number of cycles. The sample selected for the test was 90s_2.475A and the electrolytic solution was 1 M NaOH. To obtain as many cycles as possible, the potential range of chronopotentiometry test was decreased to 0.7 V (from -0.9 V to -0.2 V). In this way it was possible to reach 8000 cycles (charge-discharge) faster.

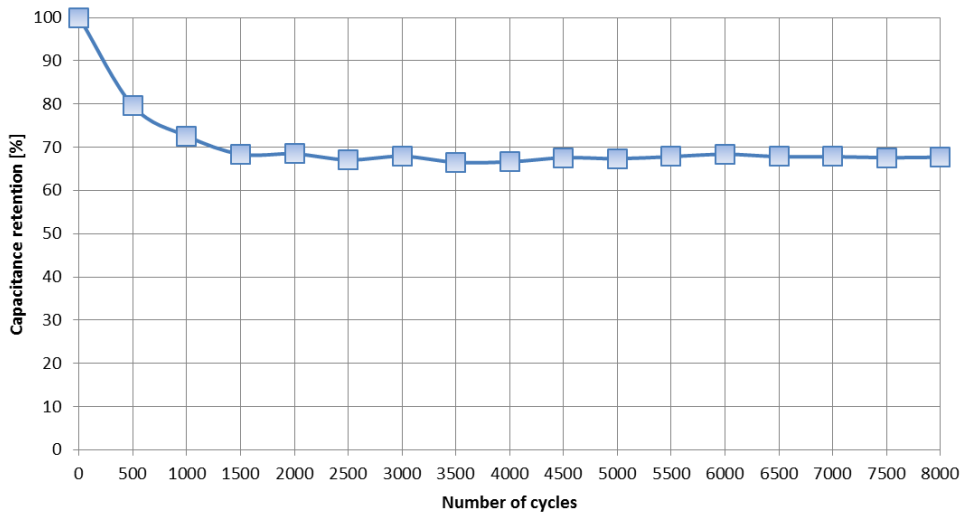

Fig. 34. Capacitance dependency on number of cycles (vs. SCE).

As can be seen from Fig. 34, the specific capacitance decreased by approximately 33.5 % until the 2500 cycle, stabilizing after that. From this moment the capacitance values stay more or less at the same level. The values obtained in this test show stability of the produced foams, which is a very important requirement for being used as electrodes for supercapacitors along with the number of charge-discharge cycles (as shown in Tab. 1.).

8. Conclusions

The objective of the present work was to develop and test nanostructured metallic Cu-Fe foams for application as Cu-Fe as electrodes for supercapacitors.

Metallic foams of Cu-Fe were produced by electrodeposition directly on stainless steel substrates that acted as the current collector.

The optimization of the electrodeposition parameters such as time and current resulted in a set of eight optimized samples, displaying the required morphology. Each sample was studied in detail using a combination of analytical and electrochemical techniques. Based on the morphology and chemical composition and electrochemical response a set of raw samples were selected: 90s_2.475A, 90s_3A and 180s_3A.

The morphological characterization of the deposited Cu-Fe foams proved, that increasing time of deposition as well as applied current can significantly change 3D foams. For sample 90s_2.475A, dispersed dendrite structures were formed over a continuous thin film composed of angular grains. The sample 90s_3A exhibited a denser network of dendritic structures, and furthermore, a network of dendritic walls was also formed. Distances between these structures for samples obtained at 90 s ranged between 15 and 20 μm. The samples prepared at 3 A and 180s (180s_3A) demonstrate honeycomb-like structure. Due to high cathodic current, deposition of Cu and Fe occurs simultaneously with intense hydrogen evolution and thus characteristic craters are created.

Morphological characterization of samples subjected to heat treatment showed, that the structure was not damaged by treatment at 150 °C or 250 °C. It was noticed, that branches of dendrites of samples treated at 250 °C are coarser than the those in the structure of raw sample or treated at 150 ºC.

The EDS analysis revealed a dependence of Cu and Fe content on the deposition parameters. Samples 90s_2.475A, 90s_3A and 180s_3A show iron contents equal 23 %, 36 % and 25 %, respectively. It means, that in order to obtain more iron in the foam structure it is crucial to limit time of deposition due to more intensified copper deposition after a period of 90 seconds. Tests on heat treated samples have shown that oxygen content has increased from 10 % (at 150 °C) to 28 % (at 250 °C).

XRD analysis provided information about planes of face-centered cubic copper and body-centered cubic iron. Diffraction patterns of sample subjected to heat treatment at 150 ºC do not differ from the diffraction patterns of raw samples. In the case of the sample treated at 250 ºC, new peak raised and corresponds to Cu_2O. The resulting diffractograms show that heat treatments lead to the partial oxidation of Cu-Fe films. Peaks related to iron oxides could not be identified, probably due to the small amount of that phase.

Cyclic voltammetry carried out in the potential window of -1.5 V to 0 V in 1 M NaOH revealed three reduction peaks and three corresponding oxidation peaks. This phenomenon is related to pseudocapacitive behavior of the deposited foams. Moreover, existing peaks correspond to Fe and Cu redox reactions what leads to a conclusion, that co-deposition of these metals occurred. Results also

showed, that the higher current, the bigger the specific area of the voltammogram. Increased specific area and intensified peaks can also be observed in the case of heat treated samples. The explanation is that heat treatment resulted in oxidation of foams present on the substrates and thus redox reactions are intensified.

The chronopotentiometric tests revealed that sample 90s_2.475A, and its heat treated correspondents, provided the best results in terms of stability. The highest specific capacitance was obtained for the 90s_2.475A_150C sample and was equal 205 Fg^{-1}. During longtime-cycle performance 8000 cycles of charge-discharge were carried out on the sample 90s_2.475A. The specific capacitance decreased by nearly 33.5 % until the 2500 cycle, stabilizing after that. The values obtained in this test showed good stability of the produced Cu-Fe foams.

Tests on Cu-Fe foams resulted in specific capacitance of 205 Fg^{-1}. This value is higher than results from other studies on Cu oxides (up to 43 Fg^{-1}) and Fe oxides (up to 100 Fg^{-1}) described in the present work (chapter 2.3.3). This can be a green light for further studies on Cu-Fe because it reveals a synergistic effect of the co-deposited metals. Moreover, the results highlight the potential of these foams in terms of using them as electrodes for supercapacitors, especially as negative electrodes in asymmetric supercapacitors.

9. Suggestions for future work

The results obtained in the present work for Cu-Fe metallic foams and their application as electrodes for supercapacitors have led to several proposals for future work:

- Heat treatment of Cu-Fe foams at higher temperatures than 250 ºC

- Optimization of electrolyte composition. For example, adjust molar concentration of sulfuric acid for better control of hydrogen bubbling and, consequently, foam porosity or Cu/Fe molar ratio in the electrolyte in order to improve Fe content in the foams

- Electrodeposition at current densities higher than 1.8 A/cm^2. During this work, the current value was limited by the equipment.

- Electrochemical tests carried out in Na_2SO_4 electrolyte.

10. Bibliography

[1] Conway B.E. (1999), Electrochemical supercapacitors: Scientific fundamentals and technological applications, Plenum Publishers

[2] Sharma P., Bhatti T.S. (2010), A review on electrochemical double-layer capacitors, Energy Conversion and Management 51, 2901-2912

[3] Shukla A.K., Banerjee A., Ravikumar M.K., Jalajakshi A. (2012), Electrochemical capacitors: Technical challenges and prognosis for future markets, Electrochimica Acta 84, 165-173

[4] Jayalakshmi M., Balasubramanian K. (2008), Simple capacitors to supercapacitors – an overview, International Journal of Electrochemical Science, 3, 1196-1217

[5] http://www.capacitorguide.com/ceramic-capacitor [accessed on September 26th 2013]

[6] Kotz R., Carlen M. (2000), Principles and applications of electrochemical capacitors, Electrochimica Acta 45, 2483-2498

[7] Zhang Y., Feng H., Wu X., Wang L., Zhang A., Xia T., Dong X., Li X., Zhang L. (2009), Progress of electrochemical capacitor electrode materials: A review, International Journal of Hydrogen Energy 34, 4889-4899

[8] Schneuwly A., Gallay R. (2000), Properties and applications of supercapacitors: from state-of-art to future trends, Presented at Power Electronics Conference

[9] Brezesinski T., Wang. J. (2010), Next generation pseudocapacitor materials from sol-gel derived transition metal oxides, Journal of Sol-Gel Science and Technology 57:330-335

[10] Nagarajan N., Zhitomirsky I. (2006), Cathodic electrosynthesis of iron oxide films for electrochemical supercapacitors, Journal of Applied Electrochemistry 36:1399-1405

[11] http://www.dla.mil [accessed on September 30th 2013]

[12] Suppes G. J. (2005), Plug-in hybrid with fuel cell battery charger, International Journal of Hydrogen Energy; 30:113–21

[13] Frackowiak E., Abbas Q., Béguin F. (2013), Carbon/carbon supercapacitors: A review, Journal of Energy Chemistry 22, 226–240

[14] Gamby J., Taberna P. L., Simon P., Fauvarque J. F., Chesnau M. (2001), Studies and characterisations of various activated carbons used for carbon/carbon supercapacitors, Journal of Power Sources 101, 109-116

[15] Obreja V. V. N. (2008), On the performance of supercapacitors with electrodes based on carbon nanotubes and carbon activated material - A review, Physica E 40, 2596–2605

[16] Snooka G. A., Kaob P., Best A. S. (2011), Conducting-polymer-based supercapacitor devices and electrodes: A review, Journal of Power Sources 196, 1–12

[17] Lokhande C.D., Dubal D.P., Joo O-S. (2011), Metal oxide thin film based supercapacitors: A review, Current Applied Physics 11, 255-270

[18] Wei J., Nagarajan N., Zhitomirsky I. (2007), Manganese oxide films for electrochemical supercapacitors, Journal of Materials Processing Technology 186, 356–361

[19] Han J., Lia L., Fang P. (2012), Ultrathin MNO2 nanorods on conducting polymer nanofibers as a new class of hierarchical nanostructures for high-performance supercapacitors, Journal of Physical Chemistry C 116:15900-15907

[20] Zhao X., Sanchez B. M., Dobson P. J., Grant P. S. (2011), The role of nanomaterials in redox-based supercapacitors for next generation energy storage devices, Nanoscale 3, 839-855

[21] Zhao D., Bao S., Zhou W., Li H. (2007), Preparation of hexagonal nanoporous nickel hydroxide film and its applications for electrochemical capacitor, Electrochemistry Communications 9, 869-874

[22] Meher S. K., Rao G. R. (2011), Ultralayered Co3O4 for high-performance supercapacitor applica-tions, Journal of Physical Chemistry C 115:15646-15654

[23] Fan Z., Chen J., Cui K., Sun F., Xu Y., Kuang Y. (2007), Preparation and capacitive properties of cobalt-nickel oxides/carbon nanotube composites, Electrochimica Acta 52, 2959–2965

[24] Wu M-S., Lee R-H. (2009), Electrochemical growth of iron oxide thin films with nanorods and nanosheets for capacitors, Journal of the Electrochemical Society 156, 9: A737-A743

[25] Wang S-Y., Ho K-C., Kuo S-L., Wu N-L. (2006), Investigation on Capacitance Mechanisms of Fe3O4 Electrochemical Capacitors, Journal of The Electrochemical Society 153 (1) A75-A80

[26] Hallam P.M., Mingot M.G., Kampouris D.K., Banks C.E. (2012), Facile synthetic fabrication of iron oxide particles and novel hydrogen superoxide supercapacitors, RSC Advances 2, 6672-6679

[27] Patake V.D., Joshi S.S., Lokhande C.D., Joob O-S. (2009), Electrodeposited porous and amorphous copper oxide film for application in supercapacitor, Materials Chemistry and Physics 114, 6–9

[28] Dubal D.P., Dhawale D.S., Salunkhe R.R., Jamdade V.S., Lockhande C.D. (2010), Fabrication of copper oxide multilayer nanosheets for supercapacitor application, Journal of Alloys and Compounds 492, 26-30

[29] Eugénio S., Silva T. M., Carmezim M. J., Duarte R. G., Montemor M. F. (2013), Electrodeposition and characterization of nickel–copper metallic foams for application as electrodes for supercapacitors, Journal of Applied Electrochemistry

[30] Shin H-C., Liu M. (2004), Copper foam structures with highly porous nanostructured walls, Chemistry of Materials 16, 5460-5464

[31] Li Y., Jia W-Z., Song Y-Y., Xia X-H. (2007), Superhydrophobicity of 3D porous copper films prepared using the hydrogen bubble dynamic template, Chemistry of Materials 19, 5758-5764

[32] Nikolic N. D., Popov K. I., Pavlovic L.J., Pavlovic M. G. (2007), Phenomenology of a formation of a honeycomb-like structure during copper electrodeposition, Journal of Solid State Electrochemistry, 11:667-675

[33] Paunovic M., Schlesinger M. (2010), Electrodeposition of iron and iron alloys, Modern Electroplating, Fifth Edition, John Wiley & Sons Incorporated

[34] Ullman's Encyclopedia of Industrial Chemistry (2006), Wiley-VCH Verlag GmbH & Co. KGaA, Weinheim

[35] Paunovic M., Schlesinger M. (2006), Fundamentals of electrochemical deposition: Second edition, John Wiley & Sons Incorporated
[36] Gamburg Y. D., Zangari G. (2011), Theory and practice of metal electrodeposition, Springer
[37] http://www.coursenotes.mcmaster.ca/4L04/Thin_Films [accessed on October 10th 2013]
[38] http://www.memsnet.org/mems/processes/deposition.html [accessed on October 18th 2013]
[39] http://serc.carleton.edu/research_education/geochemsheets/techniques [accessed on October 22nd 2013]
[40] http://www.expertsmind.com/topic/looking-at-microbes/transmission-and-scanning-electron-microscopy-92282.aspx [accessed on October 22nd 2013]
[41] Brett M.A.C., Brett M.O. (1993), Electrochemistry: Principles, methods and applications, Oxford University Press
[42] http://www.ees2.geo.rpi.edu/probe/Images/concepts/concept2.html [accessed on October 24th 2013]
[43] Bard J. A., Faulkner R. L. (2001), Electrochemical methods: Fundamentals and applications, second edition, John Wiley & Sons Incorporated
[44] Qu Q., Yang S., Feng X. (2011), 2-D sandwich-like sheets of iron oxide grown on graphene as high energy anode material for supercapacitors, Advanced materials, Volume 23: 5574-5580
[45] Matsushima H., Nohira T., Mogi I., Ito Y. (2004), Effects of magnetic fields on iron electrodeposition, Surface and Coating Technology 179, 245-251
[46] Sinapi F., Deroubaix S., Pirlot C., Delhalle J., Mekhalif Z. (2004), Electrochemical evaluation of the corrosion protection of bi-dimensional organic films self-assembled onto brass, Electrochimica Acta 49, 2987–2996
[47] Ujimine K., Tsutsumi A. (2006), Electrochemical characteristics of iron carbide as an active material in alkaline batteries, Journal of Power Sources 160, 1431–1435
[48] Geana D., El Miligy A. A., Lorenz W. J. (1974), Electrochemical behaviour of iron in Alkaline sulphate solutions, Journal of Applied Electrochemistry 4, 337-345